# DESIGN AND SYNTHESIS OF EARLY TRANSITION METAL TRIANIONIC PINCER LIGANDS

By

ADAM RAND CARLSON

A THESIS PRESENTED TO THE GRADUATE SCHOOL
OF THE UNIVERSITY OF FLORIDA IN PARTIAL FULFILLMENT
OF THE REQUIREMENTS FOR THE DEGREE OF
MASTER OF SCIENCE

UNIVERSITY OF FLORIDA

2007

To my mom

ACKNOWLEDGMENTS

I thank Dr. Adam Veige and the entire Veige Group for their support. I would also like to thank Dr. Khalil Abboud for my crystal structure data. I thank my parents for their loving encouragement, which motivated me to complete my study.

TABLE OF CONTENTS

page

ACKNOWLEDGEMENTS ..... 3

LIST OF TABLES ..... 7

LIST OF FIGURES ..... 8

LIST OF SCHEMES ..... 10

LIST OF ABBREVIATIONS ..... 11

ABSTRACT ..... 12

CHAPTER

1 INTRODUCTION ..... 13

Classic Pincer Ligands ..... 13
Features of Pincer Ligands ..... 13
Examples of Pincer Ligands in Chemistry ..... 14
Previous Trianionic Pincer Results ..... 15
Modification of NCN Trianionic Pincer Ligands and New Metallation Schemes ..... 15

2 SYNTHESIS AND REACTIONS OF $N^{C}C^{C}N$ PINCERS ..... 19

Synthesis and Characterization of [2,4,6–$MeArN^{C}C^{C}N]H_3$ (**3**) and [3,5-$CF_3N^{C}C^{C}N]H_3$ (**4**) ..... 19
Synthesis and Characterization of μ–(2,6–$^{i}$PrNCN)[$Zr(NMe_2)_3]_2$ (**6**) and [μ–(3,5–$CF_3N^{C}C^{C}N)Zr(NMe_2)_2(NHMe_2)]_2$ (**7**) ..... 20
Synthesis and Characterization of $\mu$–(3,5–$CF_3N^{C}C^{C}N)[Mo(NMe_2)_3]_2$ (**8**) ..... 21
Synthesis and Characterization of [3,5-$CF_3N^{C}C^{C}N]Mg(THF)_2$ (**10**) ..... 21
Synthesis and Characterization of [3,5–$CF_3N^{C}C^{C}N]TMS_2H$ (**11**) ..... 22
Conclusions ..... 24
Experimental ..... 24
General Considerations ..... 24
Synthesis of 2,2'-(1,3-phenylene)diethanamine (**2**) ..... 25
Synthesis of *N*,*N*'-(2,2'-(1,3-phenylene)bis(ethane-2,1-diyl)) bis(2,4,6-trimethylaniline) (**3**) ..... 25
Synthesis of *N*,*N*'-(2,2'-(1,3-phenylene)bis(ethane-2,1-diyl)) bis(3,5-bis(trifluoromethyl)aniline) (**4**) ..... 26
Synthesis of [$\mu$-(3,5–$CF_3N^{C}C^{C}N)Zr(NMe_2)_3HNMe_2]_2$ (**7**) ..... 27
Synthesis of $\mu$–(3,5–$CF_3N^{C}C^{C}N)[Mo(NMe_2)_3]_2$ (**8**) ..... 27
Synthesis of [$\mu$–(3,5–$CF_3N^{C}C^{C}N]HMg(THF)_2$ (**10**) ..... 28
Synthesis of [3,5–$CF_3N^{C}C^{C}N]H(SiMe_3)_2$ (**11**) ..... 28

page

X-ray Experimental Details For [3,5-$CF_3$-$N^CC^CN$]$H_3$ (**4**) ..... 29
X-ray Experimental Details For $\mu$–(2,6–$^i$PrNCN)[$Zr(NMe_2)_3]_2$ (**6**) ..... 30
X-ray Experimental Details For [$\mu$-(3,5–$CF_3N^CC^CN$)$Zr(NMe_2)_3HNMe_2]_2$ (**7**) .... 30
X-ray Experimental Details For [$\mu$–(3,5–$CF_3N^CC^CN$]$HMg(THF)_2$ (**10**) ..... 31

3 SYNTHESIS AND REACTIVITY OF TERPHENYL $OCO^{3-}$ PINCER COMPLEXES ..... 55

Synthesis and Characterization of terphenyl [$^t$BuOCO]$H_3$ (**17**) ..... 55
Synthesis and Characterization of [$^t$BuOCO]$MoNMe_2(HNMe_2)_2$ (**18**) ..... 56
Synthesis and Characterization of [$^t$BuOCO]MoCl (**19**) ..... 57
Conclusions ..... 58
Experimental ..... 58
General Considerations ..... 58
Synthesis of 2-bromo-6-*tert*-butylphenol (**13**) ..... 59
Synthesis of 1-bromo-3-*tert*-butyl-2-methoxybenzene (**14**) ..... 59
Synthesis of 1,3-dibromo-2-iodobenzene (**15**) ..... 60
Synthesis of 3,3”-di-*tert*-butyl-2,2”-dimethoxy-1,1’:3’,1”-terphenyl (**16**) ..... 60
Synthesis of 3,3”-di-*tert*-butyl-1,1’:3’,1” -terphenyl-2,2”-diol ([*t*BuOCO]$H_3$) (**17**) ..... 60
Synthesis of [$^t$BuOCO]$MoNMe_2(HNMe_2)_2$ (**18**) ..... 61
Synthesis of [$^t$BuOCO]$Mo(HNMe_2)_2Cl$ (**19**) ..... 62
X–ray Experimental Details For [$^t$BuOCO]$MoNMe_2(HNMe_2)_2$ (**18**) ..... 62
X–ray Experimental Details For [$^t$BuOCO]$Mo(HNMe_2)_2Cl$ (**19**) ..... 63

LIST OF REFERENCES ..... 76

BIOGRAPHICAL SKETCH ..... 79

LIST OF TABLES


Table page

2-1 Selected angles and bond lengths for crystal structures **6**, **7**, and **10** ..... 59

2-2 Crystal data, structure solution and refinement for [3,5–$CF_3N^CC^CN$]$H_3$ (**4**) ..... 51

2-3 Crystal data and structure refinement for $\mu$–(2,6–$^i$PrNCN)[$Zr(NMe_2)_3]_2$ (**6**) ..... 52

2-4 Crystal data and structure refinement for [μ-(3,5–$CF_3N^CC^CN$)$Zr(NMe_2)_3HNMe_2]_2$ (**7**) ..... 53

2-5 Crystal data and structure refinement for [$\mu$–(3,5–$CF_3N^CC^CN$]$HMg(THF)_2$ (**10**) ..... 54

3-1 Selected angles and bond lengths for crystal structures **18** and **19** ..... 73

3-2 Crystal data and structure refinement for [$^t$BuOCO]$MoNMe_2(HNMe_2)_2$ (**18**) ..... 74

3-3 Crystal data and structure refinement for [$^t$BuOCO]$Mo(HNMe_2)_2Cl$ (**19**) ..... 75

LIST OF FIGURES


| Figure | | page |
|---|---|---|
| 1-1 | Format of classic pincer ligands | 17 |
| 1-2 | Pincer catalyzed reactions | 17 |
| 1-3 | Monoanionic "Soft-Hard-Soft" and trianionic "Hard-Hard-Hard" pincer binding motifs. | 17 |
| 1-4 | POV-ray diagram of 2,6–$^{i}$PrArNCN-**Zr** and 2,6–$^{i}$PrArNCN-**Ti** | 18 |
| 2-1 | ORTEP diagram of [3,5–$CF_3N^CC^CN$]$H_3$ (**4**) | 34 |
| 2-2 | ORTEP diagram of (2,6-$^{i}$Pr-NCN)[$Zr(NMe_2)_3]_2$ (**6**) | 35 |
| 2-3 | ORTEP diagram of $\mu$-(3,5–$CF_3$-$N^CC^CN$)[$Zr(NMe_2)_2(HNMe_2)]_2$ (**7**) | 36 |
| 2-4 | ORTEP diagram of [$\mu$–(3,5–$CF_3N^CC^CN$]$HMg(THF)_2$ (**10**) | 37 |
| 2-5 | $^{1}$H NMR spectra of 2,2'-(1,3-phenylene)diethanamine (**2**) in $C_6D_6$ | 38 |
| 2-6 | $^{1}$H NMR spectra of [2,4,6-Me$N^CC^CN$]$H_3$ (**3**) in $C_6D_6$ | 39 |
| 2-7 | $^{1}$H NMR spectra of [3,5-$CF_3N^CC^CN$]$H_3$ (**4**) in $C_6D_6$ | 40 |
| 2-8 | $^{13}C\{^{1}H\}$ NMR spectrum of [3,5-$CF_3N^CC^CN$]$H_3$ (**4**) in $C_6D_6$ | 41 |
| 2-9 | $^{1}$H NMR spectra of [$\mu$-(3,5–$CF_3N^CC^CN$)$Zr(NMe_2)_3HNMe_2]_2$ (**7**) in $C_6D_6$ | 42 |
| 2-10 | $^{13}C\{^{1}H\}$ NMR spectrum of [$\mu$-(3,5–$CF_3N^CC^CN$)$Zr(NMe_2)_3HNMe_2]_2$ (**7**) in THF-$d_8$ | 43 |
| 2-11 | $^{1}$H NMR spectra of $\mu$–(3,5–$CF_3N^CC^CN$)[$Mo(NMe_2)_3]_2$ (**8**) in $C_6D_6$ | 44 |
| 2-12 | $^{13}C\{^{1}H\}$ NMR spectrum of $\mu$–(3,5–$CF_3N^CC^CN$)[$Mo(NMe_2)_3]_2$ (**8**) in $C_6D_6$ | 45 |
| 2-13 | $^{1}$H NMR spectra of [3,5-$CF_3N^CC^CN$]$HMg(THF)_2$ (**10**) in Tol-$d_8$ @ -75 °C | 46 |
| 2-14 | $^{1}$H NMR spectra of [3,5–$CF_3N^CC^CN$]$H(SiMe_3)_2$ (**11**) in $C_6D_6$ | 47 |
| 2-15 | $^{13}C\{^{1}H\}$ NMR spectrum of [3,5–$CF_3N^CC^CN$]$H(SiMe_3)_2$ (**11**) in $C_6D_6$ | 48 |
| 2-16 | $^{19}$F NMR spectrum of [3,5–$CF_3N^CC^CN$]$H(SiMe_3)_2$ (**11**) in $C_6D_6$ | 49 |
| 3-1 | ORTEP diagram of [$^{t}$BuOCO]$MoNMe_2(HNMe_2)_2$ (**18**) | 65 |

Figure page

3-2 ORTEP diagram of [$^{t}$BuOCO]Mo(HNMe$_2$)$_2$Cl (**19**) ..... 66

3-3 $^{1}$H NMR spectrum of [$^{t}$BuOCO]H$_3$ (**17**) in acetone-*d*$_6$ ..... 67

3-4 $^{13}$C NMR spectrum of [$^{t}$BuOCO]H$_3$ (**17**) inC$_6$D$_6$ ..... 68

3-5 $^{1}$H NMR spectrum of [$^{t}$BuOCO]MoNMe$_2$(HNMe$_2$)$_2$ (**18**) in THF-*d*$_8$ ..... 69

3-6 $^{13}$C NMR spectrum of [$^{t}$BuOCO]MoNMe$_2$(HNMe$_2$)$_2$ (**18**) in THF-*d*$_8$ ..... 70

3-7 $^{1}$H NMR spectrum of [$^{t}$BuOCO]Mo(HNMe$_2$)$_2$Cl (**19**) in C$_6$D$_6$ ..... 71

3-8 $^{13}$C NMR spectrum of [$^{t}$BuOCO]Mo(HNMe$_2$)$_2$Cl (**19**) in THF-*d*$_8$ ..... 72

LIST OF SCHEMES


| Scheme | | page |
|---|---|---|
| 1-1 | Formation of group 4 NCN metal complexes | 16 |
| 1-2 | Metallation via trimethylsilyl-halide elimination | 16 |
| 1-3 | Metallation via amine extrusion | 16 |
| 2-1 | Synthesis of $ArN^{C}C^{C}NH_3$ (where Ar = 2,4,6-$MeC_6H_3$ (**3**) and 3,5–$CF_3C_6H_3$ (**4**)) | 32 |
| 2-2 | Synthesis of **6** and **7** (where Ar = 2,4-$^{i}PrC_6H_3$ (**6**) and 3,5–$CF_3C_6H_3$ (**7**) | 32 |
| 2-3 | Synthesis of the molybdenum dinuclear species $\mu$–(3,5–$CF_3N^{C}C^{C}N$)[$Mo(NMe_2)_3]_2$ (**8**) | 33 |
| 2-4 | Synthesis of the dimagnesio salt [3,5–$CF_3N^{C}C^{C}N$]H[$MgCl(THF)_2]_2$ (**9**) and the minor impurity monomagnesio salt [$\mu$–(3,5–$CF_3N^{C}C^{C}N$]$HMg(THF)_2$ (**10**) | 33 |
| 2-5 | Synthesis of the bistrimethylsilyl species [3,5–$CF_3N^{C}C^{C}N$]$H(SiMe_3)_2$ (**11**) | 33 |
| 3-1 | Synthesis of [$^{t}$BuOCO]$H_3$ (**17**) | 64 |
| 3-2 | Synthesis of [$^{t}$BuOCO]$MoNMe_2(HNMe_2)_2$ (**18**) | 64 |
| 3-3 | Synthesis of [$^{t}$BuOCO]$Mo(HNMe_2)_2Cl$ (**19**) | 65 |

# LIST OF ABBREVIATIONS

| | |
|---|---|
| ECE | electron donor-carbon-electron donor pincer ligands |
| $e^-$ | electron |
| M-C | a metal-carbon bond |
| $^{i}$Pr | *iso*-propyl |
| $^{t}$Bu | *tert*-butyl |
| EDG | electron donating group |
| EWG | electron widthdrawing group |
| PCP | phosphorous-carbon-phosphorous |
| NCN | nitrogen-carbon-nitrogen pincer ligands |
| OCO | oxygen-carbon-oxygen pincer ligand |
| NMR | nuclear magnetic resonance |
| HRMS | high resolution mass spectrometry |

Abstract of Thesis Presented to the Graduate School
of the University of Florida in Partial Fulfillment of the
Requirements for the Degree of Master of Science

DESIGN AND SYNTHESIS OF EARLY TRANSITION METAL
TRIANIONIC PINCER LIGANDS

By

Adam Rand Carlson

December 2007

Chairman: Adam Veige
Major: Chemistry

The chemistry of trianionic pincer ligands is largely unknown, but preliminary synthetic studies establish their terdentate coordination behavior. Early transition metals differ greatly in reactivity and coordination compared with late transition metals. Classic pincer ligands have been designed for use with "soft" late transition metals and are not well suited for early transition metals. New trianionic pincer ligands utilize a "hard-hard-hard" binding motif, which is more suitable for "hard" early transition metals. Appropriate conditions for coordination of trianionic pincer ligands to early transition metals must be developed. Pincer ligands are easily modified and are not limited to a single method of metallation. This thesis describes the synthesis and reactivity of new trianionic pincer ligands $NCN^{3-}$ and $OCO^{3-}$ with group 4 and 6 early transition metals.

# CHAPTER 1
# INTRODUCTION

## Classic Pincer Ligands

The first mention of a pincer ligand in the literature was by Shaw in 1976. He described a PCP pincer review coordinated to rhodium(III), iridium(III), palladium(II) and platinum(II) (group 9 and 10) metal ions.[1-5] Pincer ligated metal complexes, when used in homogeneous metal catalysis, can promote efficient chemical transformations. Today these complexes are used with great success in a wide range of industrial and fine chemical syntheses.[6-13]

## Features of Pincer Ligands

Pincer ligands share two salient features, the most important being the presence of a central metal-aryl σ-bond. This metal-carbon (M-C) bond renders complexes thermally robust and prevents dissociation from the metal even at high temperatures, leading to high turnover numbers. This M-C bond carries a single negative charge, making the majority of pincer ligands monoanionic.

The second characteristic of classic pincer ligands is the presence of two neutral, two electron donor atoms attached via methylene spacers at the 2- and 6-positions of the aryl backbone. Tertiary phosphines such as those first used by Shaw were initially used as donor atoms, but the incorporation of other neutral $2e^-$ donors (Figure 1-1) into the structure has led to the complexation of a wide range of transition metals.[14] These two electron donors are typically denoted as "E", making the abbreviation for pincer ligands "ECE". The pendant arms can be altered to enable control of electron density at the metal. The terdentate binding of a pincer ligand to metals increases the stability of the organometallic complex relative to mono or bidentate ligands. The terdentate motif also serves to enable greater control over accessibility to the metal, and therefore substrate binding, since the ligand occupies three coordination sites.

Further tailoring of this modular architecture by the addition of electron withdrawing (EWG) or electron donating (EDG) groups to the aryl backbone can fine-tune the electron density at the metal.[15]

## Examples of Pincer Ligands in Chemistry

The variety of chemical transformations that can be catalyzed by pincer ligand systems is beyond the scope of this thesis[16] but a few examples are shown below (Figure 1-2).[17,18] These reactions include poly-olefin,[19] alkane and cycloalkane dehydrogenation, Suzuki couplings,[20] Heck reactions, aldol reactions, cyclopropanations, allylation of alcohols, allylic alkylation, hydrogenation of ketones, Kharasch additions,[21] and Michael reactions.

To date the majority of useful pincer related catalysts have used the expensive late metals. The main objective for this project is to tailor a pincer ligand so that it will accommodate the specific demands of cheaper early transition metals. The problem with using a classic pincer ligand design to form an early transition metal complex, is that early and late transition metals differ significantly in their properties. Generally, late transition metals favor low oxidation states, are low coordinate and are tolerant of many functional groups.[22-25] By contrast, early transition metals favor high oxidation states and are intolerant of many functional groups. In a classic pincer ligand, the interaction between the pendant arms and the metal is a lone-pair donation, considered as a "soft" delocalized interaction. By comparison, the anionic carbon is considered "hard" giving classic pincer ligands a "soft-hard-soft" interaction with a metal center. This is ideal for late transition metals, which are considered "soft", but the interaction is not preferred by early transition metals, which are considered "hard".

The hard nature of the early transition metals necessitates modification of the pincer ligand from its traditional monoanionic "soft-hard-soft" design to a trianionic "hard-hard-hard"

binding motif (Figure 1-3). This hard donation can be accomplished via a localized electron pair donation of an anionic "hard" atom such as $C^-$, $N^-$, or $O^-$. Because early transition metals are electro-positive this hard interaction stabilizes higher oxidation states. A trianionic pincer ligand serves to occupy three coordination sites of the metal and at least stabilize oxidation state of $3^+$. As with late transition metal pincer systems a halide *trans* to the M-C bond serves to promote functionalization of the complex, or allow for entry into various catalytic cycles. This halide contributes to produce a $4^+$ oxidation state with a trianionic pincer ligand. The $4^+$ oxidation state is common for our target group 4 and 6 metals.

**Previous Trianionic Pincer Results**

The first generation trianionic pincer ligands successfully ligated all of the group 4 metals (Ti, Zr, Hf) by using a trilithio salts of the parent NCN ligand **(**Scheme 1-1). However, when applied to group 6 metals only intractable mixtures were produced. This was presumably due to electron-transfer reduction of the metal substrate. Early transition metals are especially susceptible to these side reactions during R-Li salt metathesis. X-ray crystal structures of the group 4 metal-NCN complexes did reveal very small N-M-N bond angles of ~140º (Figure 1-4) compared with N-M-N bond angles of ~160º for late transition metals.[26-27] Based on these results we sought to make a change to the NCN pincer design, and explore alternative routes to metallation.

**Modification of NCN Trianionic Pincer Ligands and New Metallation Schemes**

The first change needed was an increase in the length of the pendant arms from single methylene spacers. Inserting an additional methylene spacer to form $N^CC^CN$ derivatives would produce two six-membered rings once chelated, but more importantly would allow for changes in metal atomic radii during reaction sequences. The second change was a modification of our

approach to metallation. One of the benefits of using hard donor atoms is the ease of functionalization thus enabling different metallation schemes. The donor atoms can be modified to include functional groups such as $SiMe_3$, which have been shown to eliminate trimethylsilylhalides when reacted with metal halides.[28] This method serves to chelate the metal followed by stepwise alkylation of the metal that can form the final M-C bond (Scheme 1-2). While lithium salts were used successfully to ligate group 4 metals sodium and potassium salts are an alternative for group 6 metals. In addition, protonated ligands can be reacted directly with metal dialkylamides which eliminates dialkylamine (Scheme 1-3).

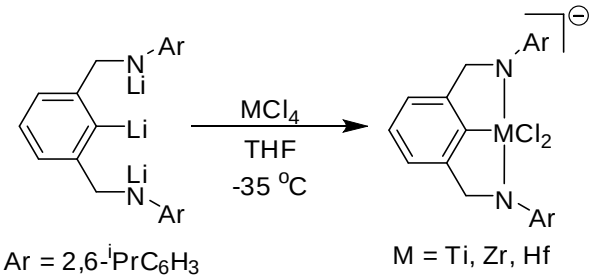


Scheme 1-1. Formation of group 4 NCN metal complexes.

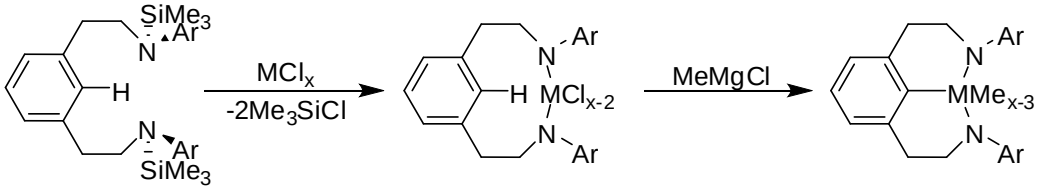


Scheme 1-2. Metallation via trimethylsilyl-halide elimination.

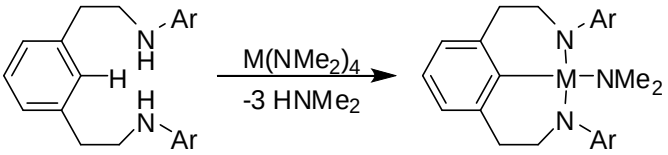


Scheme 1-3. Metallation via amine extrusion.

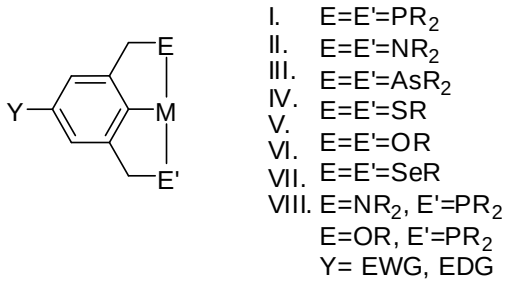


Figure 1-1. Format of classic pincer ligands.

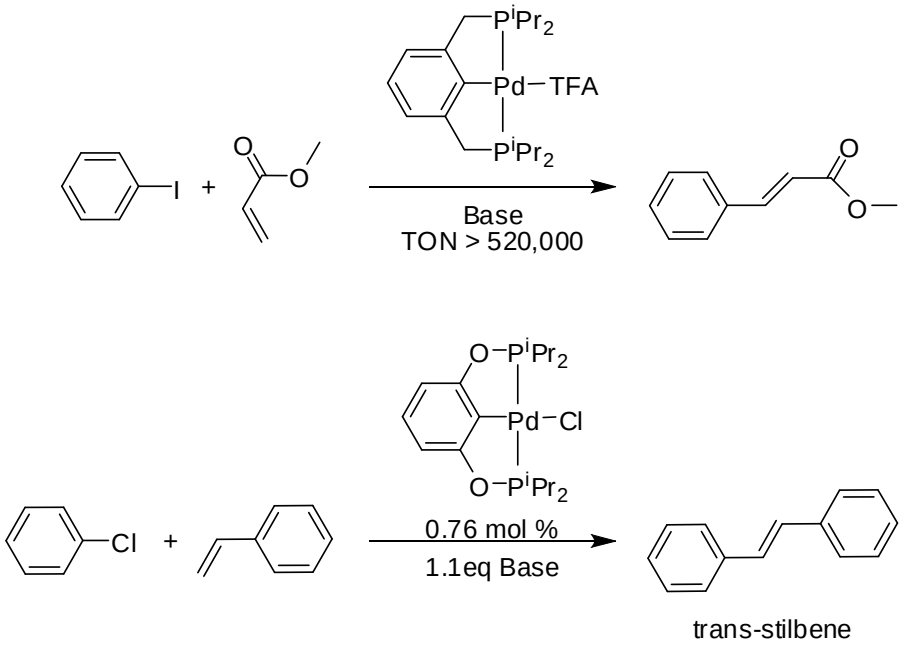


Figure 1-2. Pincer catalyzed reactions.

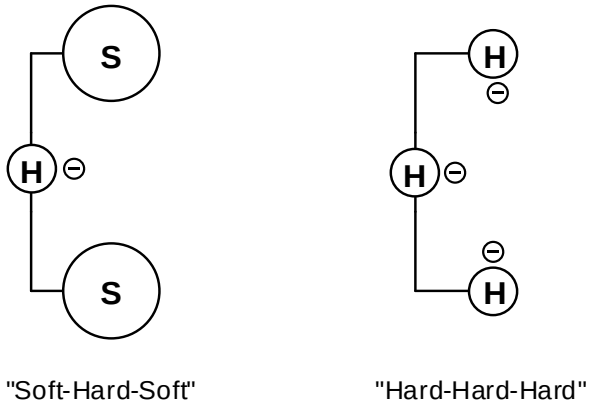


Figure 1-3**.** Monoanionic "Soft-Hard-Soft" and trianionic "Hard-Hard-Hard" pincer binding motifs.

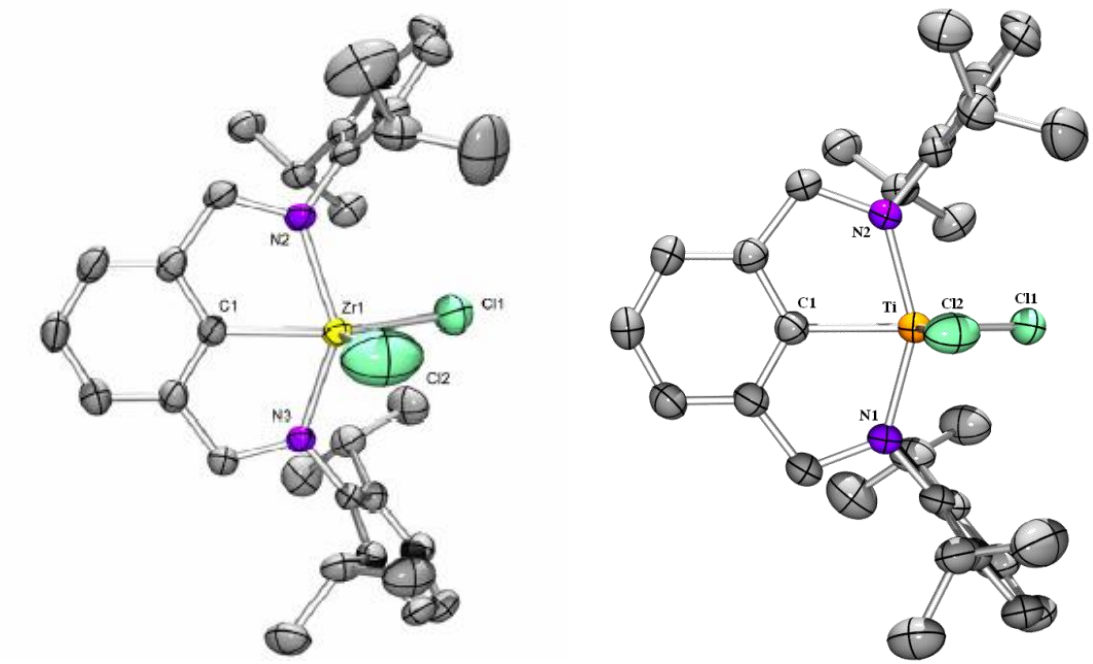


Figure 1-4. POV-ray diagram of 2,6–$^{i}$PrArNCN-**Zr** and 2,6–$^{i}$PrArNCN-**Ti.**
Selected bond angles; N2-Zr-N1 = 140.11°, N1-Ti-N2 = 144.46°

# CHAPTER 2
# SYNTHESIS AND METALLATION OF $N^{C}C^{C}N$ PINCER LIGANDS

## Synthesis and Characterization of [2,4,6–MeAr$N^{C}C^{C}N$]$H_3$ (3) and [3,5-$CF_3N^{C}C^{C}N$]$H_3$ (4)

The most direct synthesis of our target $N^{C}C^{C}N$ pincer ligands utilizes diamine **2**. This starting material allows for easy access to a variety of pincer ligands via cross-coupling with any commercially available bromobenzene. Diamine **2** is not commercially available, but can be synthesized by reduction of dicyano **1** with $LiAlH_4$.[29] Diamine **2** was obtained in 33% yield following purification by distillation. The identity of **2** was verified by $^1$H NMR spectroscopy. The two sets of methylene protons are observed as triplets that integrate to four protons each and appear at 2.88 and 2.65 ppm. A corresponding broad singlet is observed at 1.01 ppm and is ascribed to the two NH protons. Diamine **2** was then used in a Buchwald-Hartwig cross-coupling reaction[30,31] with 1-bromomesitylene or 3,5-trifluoromethylbromobenzene to produce ligand **3** and **4** in 61% and 33% yield respectively (Scheme 2-1).

A $^1$H NMR spectrum of **3** revealed the expected two sets of methylene protons as a doublet of triplets at 3.08 ppm and a triplet at 2.80 ppm. The key feature of the spectrum for **3** are two singlets corresponding to the methyl groups in the 2, 4, and 6 positions which and appear at 2.15 and 2.06 ppm in a 6:12 ratio respectively.

The $^1$H NMR spectrum of **4** is similar, as expected to **3**. A doublet of triplets and triplet at 3.73 and 2.38 ppm are observed for the two sets of methylene protons. The most indicative peak of the molecule is a singlet at 6.48 ppm corresponding to the four protons in the 2 and 6 positions of the trifluoromethyl aryl rings. The unique position of this peak is used to monitor the progression of metallation reactions. Although ligand **3** is as an oil, **4** is easily crystallized from saturated pentane solutions. The increased crystallinity of **4** can be attributed to the trifluoromethyl groups. The molecular structure, determined by X-ray crystallography is

presented in Figure 2-1 and shows a staggered π-stacking arrangement of three trifluoromethyl rings from two independent ligand molecules. A table of pertinent bond lengths and angles is presented in Table 2-1. The combined spectroscopic analysis and X-ray experiment confirmed the identity of **4**.

### Synthesis and Characterization of $\mu$–(2,6–$^{i}$PrNCN)[Zr(NMe$_2$)$_3$]$_2$ (6) and [$\mu$–(3,5–CF$_3$N$^{C}$C$^{C}$N)Zr(NMe$_2$)$_2$(NHMe$_2$)]$_2$ (7)

Previous work in the Veige group was centered on the NCN derivative **5** in which only one methylene group is present in the pincer arm. When **5** is treated with Zr(NMe$_2$)$_4$ the bimetallic complex **6** is formed (Scheme 2-2) which was characterizaed by X–Ray crystallographyand the structure is presented in Figure 2–2. The zirconium remains in a tetrahedral geometry with three coordination sites occupied by dimethylamide ligands. In contrast ligation of Zr(NMe$_2$)$_4$ with **4** produced dimer **7** in which each ligand occupies an axial and equatorial site of opposing metal centers. The molecular structure is presented in Figure 2-3**.** One coordinated dimethylamide group remains and is located *trans* to the ligand amide bond. The coordinated dimethylamine is distinguished from the amides by its tetrahedral geometry and the remaining amides are planar. The zirconium center has a distorted trigonal bipyramidal geometry, with the equatorial amides separated by 114.44(11)° to 122.10(10)° and the axial nitrogen atoms lying 174.00(10)° apart (Table 2-1).

Although ligand **4** did not chelate the metal as hoped, some information was obtained from the difference in reactivity between **4** and **5**. Clearly by moving the alkyl groups to the 3,5 positions allowed for the formation of a symmetric dimer that contained two bridging ligands whereas the sterically bulky $^{i}$Pr groups only allowed one ligand to bridge. The influence of alkyl group size in reactions with Zr(NMe$_2$)$_4$ was also probed by Lappert and coworkers.[32] A

compound analogous to **6,** with 2,6-methyl groups was reported to dimerize and incorporate two bridging ligands under similar reaction conditions.

### Synthesis and Characterization of $\mu$–(3,5–$CF_3N^CC^CN$)[$Mo(NMe_2)_3$]$_2$ (8)

Additional reactivity differences between **4** and **5** are observed when treated with $Mo(NMe_2)_4$. Ligand **5** proved unreactive, even when heated to reflux in toluene for 18 hours. The lack of reactivity with $Mo(NMe_2)_4$ is due to proximity and size of the 2,6–$^i$Pr groups. By comparison, treatment of **4** with $Mo(NMe_2)_4$ resulted in coordination of the amide groups to Mo. While less than 2.5 equiv of $Mo(NMe_2)_4$ did not consume all of **4**, a bimetallic product could by detected by $^1$H NMR spectroscopy when 3 equivalents were employed (Scheme 2-3). After heating the reagents at 40 °C for 4 d a product was isolated by removal of all volatiles *in vacuo* and then subliming the remaining $Mo(NMe_2)_4$. The product is tentatively assigned as the bimetallic complex $\mu$–(3,5–$CF_3$NCN)[$Mo(NMe_2)_3$]$_2$ **(8)** and is characterized by $^1$H NMR spectroscopy. The two sets of methylene protons appear as triplets at 3.73 and 2.84 ppm. A large singlet at 3.08 ppm that integrates to 36 protons is assigned to the methyl protons of 6 equivalent dimethylamide ligands. This supports the assignment of two molybdenum atoms that coordinate 3 equivalent dimethylamides each, as in the crystallographically determined structure of **6** above.

### Synthesis and Characterization of [3,5-$CF_3N^CC^CN$]$Mg(THF)_2$ (10)

To avoid the slow reactivity with metal dialkylamides we investigated a trimethylsilylhalide (TMSX) elimination route. By attaching TMS groups to the nitrogen atoms of **4** we hoped to eliminate TMSX from metal halide precursors which are commercially available and offer abundant variations with respect to choice of transition metal and oxidation state. The first step in creating TMS derivatives of **4** requires the synthesis of a dimagnesio salt,

which led to an interesting observation. When **4** is treated with MeMgCl and after removal of THF the chelated magnesium product [3,5-$CF_3N^CC^CN$]$Mg(THF)_2$ (**10**) was extracted with pentane and single crystals were obtained (Scheme 2-4). This *N*,*N*-chelated product is a side product and is only obtained in a minimal yield, however, enough was isolated to enable both low temperature $^1$H NMR spectroscopy and X-ray structure determination.

The X-ray structure (Figure 2-4) obtained at 173 K indicates that the magnesium is oriented such that the *ipso*-aryl C-H bond is positioned directly over the metal center. The tetrahedral coordination sphere is comprised of the two amides from the ligand and two oxygen atoms from coordinated THF molecules. After chelation of the amides it is apparent that the ligand is in the correct conformation for C-H activation by a metal. This result provides insight into a potential metallation route in which the arms first attach and then the backbone C–H bond is activated. While this confirms pendant arm chelation as a possible route to installing trianionic ligands on target metals the magnesium in this complex is unable to accomplish this as it is lacks an accessible higher oxidation state. In the $^1$H NMR spectrum the protons in the coordinated THF molecules are shifted 0.5 ppm upfield. The methylene and coordinated THF protons are fluxional on the NMR time scale resulting in their appearance as broad peaks at ambient temperature. As the temperature is reduced to –75 °C the protons in the ligand methylene groups begin to resolve away from the THF protons. Unfortunately the low yield of **10** prevented further investigation and the synthesis of the [3,5–$CF_3N^CC^CN$]$TMS_2H$ (**11**) was conducted by *in situ* preparation of a dimagnesio salt.

### Synthesis and Characterization of [3,5–$CF_3N^CC^CN$]$TMS_2H$ (11)

The *N*,*N*-TMS derivative **11** was formed by treating **4** with 2.1 equiv of methyl Grignard, followed by addition of 3 equiv of TMSCl. **11** is obtained as a white crystalline solid in 74%

yield (Scheme 2-5). The $^{1}$H NMR spectrum of **11** revealed the expected signals for the methylene groups and the singlet from the *ortho*–aryl protons formerly at 6.48 ppm for ligand **4** shifted to 7.35 ppm. The prominent feature of the spectra is the singlet at 0.00 ppm which is assigned to the six methyl groups from two trimethylsilyls. Integration of the singlet from the TMS groups only indicates fifteen protons, rather than the expected eighteen. This can be attributed to a difference in relaxation times for these protons though they were not determined and the identity of **11** was confirmed by additional means. $^{19}$F NMR shows only one sharp singlet at -63.32, indicating only one compound is formed and a $^{13}$C NMR spectrum indicated the presence of twelve peaks, the largest attributed to the $SiMe_3$ carbons at 0.75 ppm.

Ligand **11** was treated with $TiCl_4$, $ZrF_4$, $TaF_5$, $ZrI_4$, and $MoCl_5$ in refluxing toluene or xylenes for 12-24 hr periods. The $^{1}$H NMR spectrum of the $ZrF_4$ reaction mixture showed only **11** even after 20 hrs in refluxing xylenes, indicative of the thermal stability of the ligand. Reactions with $TaF_5$, $ZrI_4$, and $MoCl_5$ gave products whose NMR spectra were consistent with the parent ligand **4**. This occurred even after care was taken to silylate all glass surfaces to reduce the likelihood that protons were coming from the glassware. The presence of TMSI and TMSCl in the $^{1}$H NMR spectra indicated that the ligand was reacting with metal halides, but was not anchoring via C–H bond activation of the backbone. Only reactions with $TiCl_4$ showed the presence of a product (in the $^{1}$H NMR spectra up to 33%). The $^{1}$H NMR spectra showed new peaks attributed to the two pairs of methylene protons at 3.72 and 2.55 ppm. The position of these suggests a new product was formed with titanium. The product was never isolated and pale yellow crystals were grown but deteriorated before X-ray analysis could be conducted.

## Conclusions

Metallation attempts with ligand **4** revealed two problems. Lack of rigidity promotes dimerization and sterics force the two pendant arms apart. This is further complicated by slow reactivity in aminolysis reactions. Without a driving force to chelate a single metal or without the pendant arms being forced together, ligand **4** has an affinity for dimerization. The TMS-halide elimination metallation route has similar drawbacks. While metal chelated pincers are very robust, the high temperatures used to promote reactions of **11** with metal halides ultimately lead to N-M bond protonation. While this remains a viable route to metallation, it will require additional modification of the NCN ligand.

## Experimental

### General Considerations

Unless specified otherwise, all manipulations were performed under an inert atmosphere using standard Schlenk or glovebox techniques. Pentane, hexanes, toluene, diethyl ether, tetrahydrofuran, and 1,2–dimethoxyethane were dried using a GlassContour drying column. $C_6D_6$ and toluene-$d_8$ (Cambridge Isotopes) were dried over sodium–benzophenone ketyl, distilled or vacuum transferred and stored over 4 Å molecular sieves. THF-$d_8$ (Cambridge Isotopes) was stored over 4 Å sieves and used without further purification. Sublimed $Zr(NMe_2)_4$ was purchased from Strem Chemicals and used without further purification. $LiAlH_4$ (95%), m-xylylenedicyanide (99%), and 2-bromomesitylene (99%), were purchased from Acros and used as received. $Pd_2(dba)_3$, 3,5-bis(trifluoromethyl)bromobenzene, MeMgCl (3.0 M in THF), and chlorotrimethylsilane (97%) were purchased from Aldrich and used as received. *rac*-BINAP was purchased from Fluka and used as received. $Mo(NMe_2)_4$ was synthesized according to the procedure from Chisholm *et al*.[33]

NMR spectra were obtained on Gemini (300 MHz), VXR (300 MHz), or Mercury (300 MHz) spectrometers. Chemical shifts are reported in δ (ppm). For $^{1}H$ and $^{13}C$ NMR spectra, the residual protio or carbon solvent peak were referenced as an internal reference. GC/MS spectra were recorded on an Agilent 6210 TOF–MS instrument. C, H, and N elemental analysis were determined by Robertson Microlit Laboratories Inc. and Complete Analysis Laboratories.

**Synthesis of 2,2'-(1,3-phenylene)diethanamine (2)**

An alternative synthesis of **2** was performed.[34] Under argon flow diethyl ether (500 mL) was added to $LiAlH_4$ (60 g, 12.7 equiv, 1.58 mmol) in a 1000 mL three-neck flask fitted with a reflux condenser, a 500 mL dropping funnel and a stirbar. To the dropping funnel was added *m*-xylylene dicyanide (**1**) (19.4 g, 0.124 mol) in diethyl ether (300 mL). The *m*-xylylene dicyanide solution was added dropwise under static argon over a period of 2 h with vigorous stirring and then refluxed for 48 h. The resulting green suspension was cooled to 0 °C and then water (100 mL) was added dropwise through the dropping funnel, followed by a 15% by wt. solution of NaOH (100 mL). Extra diethyl ether was added periodically. An additional 30 mL of water was added to produce a free-flowing white suspension. Compound **2** was extracted from the white suspension with diethyl ether (6 x 150 mL) and each portion was dried over $Na_2SO_4$ then condensed *in vacuo* and combined. The transparent yellow oil was purified by distillation at 170 °C @ 20 mTorr. Yield 6.0 g (0.036 mol, 39.0%). $^{1}H$ NMR (300 MHz, $C_6D_6$, δ): 7.15 (t, $J$ = 7.30 Hz, 1H, Ar H), 6.99 (s, 1H, Ar H), 6.97 (s, 2H, Ar H), 2.88 (t, $J$ = 6.86 Hz, 4H, -$NH_2$-C$H_2$), 2.65 (t, $J$ = 6.86 Hz, 4H, -C$H_2$-Ar), 1.01 (br. s, 4H, N$H_2$).

**Synthesis of *N*,*N*'-(2,2'-(1,3-phenylene)bis(ethane-2,1-diyl))bis(2,4,6-trimethylaniline) (3)**

To a 100 mL round bottom flask charged with a stir bar and toluene (50 mL) were added 2 (0.920 g, 5.61 mmol), 2-bromomesitylene (2.230 g, 2 equiv, 11.22 mmol), $Pd_2(dba)_3$ (0.080 g,

0.5%, 0.087 mmol), *rac*-BINAP (0.140 g, 1.5%, 0.219 mmol), and NaO$^t$Bu (1.617 g, 16.83 mmol). After refluxing for 72 h under argon the solution was filtered through celite while hot and the remaining toluene was removed *in vacuo*. Nonvolatile products were then taken up in hot pentanes and filtered again through celite. The final product was produced as a light red oil after volatiles were removed *in vacuo*. Yield 1.36 g (3.4 mmol, 61%). $^1$H NMR (300 MHz, $C_6D_6$, δ): 7.14 (s, 1H, *ipso*-Ar H), 7.08 (t, *J* = 7.61 Hz, 1H, Ar H), 6.91 (d, *J* = 5.97 Hz, 2H, Ar H), 6.75 (s, 4H, Ar H), 3.08 (dt, *J* = 6.86 Hz, *J* = 0.86 Hz, 4H, N-C*H*$_2$-), 2.80 (t, *J* = 7.01 Hz, 2H, NH), 2.63 (t, *J* = 6.86 Hz, 4H, Ar-C*H*$_2$-), 2.15 (s, 6H, Ar-4-C*H*$_3$), 2.06 (s, 12H, Ar-2,6-C*H*$_3$).

**Synthesis of *N*,*N*'-(2,2'-(1,3-phenylene)bis(ethane-2,1-diyl))bis(3,5-bis(trifluoromethyl)aniline) (4)**

To a 100 mL round bottom flask charged with a stir bar and toluene (50 mL) were added **2** (1.500 g, 9.15 mmol), 3,5-bis(trifluoromethyl)bromobenzene (5.370 g, 2 equiv, 18.3 mmol), $Pd_2(dba)_3$ (0.130 g, 0.5%, 0.142 mmol), *rac*-BINAP (0.228 g, 1.5%, 0.357 mmol), and NaO$^t$Bu (2.637 g, 27.5 mmol). After refluxing for 72 h under argon the solution was filtered through celite while hot and the remaining toluene was removed *in vacuo*. Nonvolatile products were then taken up in hot pentanes and filtered through celite again. The final product was recrystallized two times in pentane at -20 °C. Yield 2.1 g (3.57 mmol, 39.0%). $^1$H NMR (300 MHz, $C_6D_6$, δ): 7.22 (s, 2H, Ar H), 7.11 (t, *J* = 7.64 Hz, 1H, Ar H), 6.81 (dd, *J* = 7.64, 1.70 Hz, 2H, Ar H), 6.72 (s, 1H, Ar H), 6.48 (s, 4H, Ar H), 3.13 (t, *J* = 5.52 Hz, 2H, NH), 2.73 (dt, *J* = 6.94 Hz, 4H, NH-C*H*$_2$-), 2.38 (t, *J* = 6.94 Hz, 4H, -C*H*$_2$-Ar). $^{13}$C{$^1$H} NMR (128.39 Hz, $C_6D_6$, δ): 35.35 (s, -*C*H$_2$-Ar), 44.62 (s, -HN-*C*H$_2$-), 110.38 (s, aromatic), 112.27 (s, aromatic), 122.85 (s, aromatic), 126.47 (s, aromatic), 127.60 (s, aromatic), 129.71 (s, aromatic), 132.97 (q, *J* = 32.74 Hz, -*C*F$_3$), 139.76 (s, Ar*C*-CH$_2$-), 149.16 (s, Ar*C*-NH-). HRMS calculated (found) for $C_{26}H_{20}F_{12}N_2$ (M+H$^+$) 589.1508 (589.1537).

**Synthesis of [$\mu$-(3,5–$CF_3N^CC^CN$)$Zr(NMe_2)_3HNMe_2]_2$ (7)**

A solution of $Zr(NMe_2)_4$ (45 mg, 0.170 mmol) in toluene (1 mL) was added to **4** (100 mg, 0.170 mmol) in toluene (1 mL) at -35 °C with stirring. After warming to ambient temperature and stirring for 3 h, volatiles from the resulting brown solution were removed *in vacuo*. The product was recrystallized from concentrated solutions of **7** in toluene over a period of 7 days. $^1$H NMR (300 MHz, THF-$D_8$, δ): 7.39-6.98 (m, 18H (11H), Ar H), 3.78 (t, *J* = 8.49 Hz, 4H, N-C*H*$_2$-), 3.13 (s, 12H, -N(C*H*$_3$)$_2$), 2.77 (t, *J* = 7.64 Hz, 4H, Ar-C*H*$_2$-), 2.31 (s, 6H, HN(C*H*$_3$)$_2$), 2.28 (s, 1H, *H*N(CH$_3$)$_2$). $^{13}$C{$^1$H} NMR (67.57 Hz, THF-$D_8$, δ): 21.52 (s, HN(*C*H$_3$)$_2$), 35.24 (s, -N-*C*H$_2$-), 36.07 (s, -N-*C*H$_2$-), 39.36 (s, N(*C*H$_3$)$_2$), 43.04 (s, N(*C*H$_3$)$_2$), 45.57 (s, Ar-*C*H$_2$-), 50.02 (s, Ar-*C*H$_2$-), 109.57 (s, aromatic), 112.22 (s, aromatic), 115.75 (s, aromatic), 123.38 (s, aromatic), 126.08 (s, aromatic), 127.33 (s, aromatic), 128.95 (s, aromatic), 129.72 (s, aromatic), 133.30 (q, *J* = 32.0 Hz, *C*F$_3$), 141.02 (s, aromatic), 155.53 (s, aromatic). Anal. Calcd for $C_{64}H_{74}F_{24}N_{10}Zr_2$ (2 $C_6D_6$) C, 50.95; H, 4.13; N, 7.82. Found: C, 49.28; H, 4.50; N, 5.83.

**Synthesis of $\mu$–(3,5–$CF_3N^CC^CN$)$[Mo(NMe_2)_3]_2$ (8)**

To a 50 mL sealed ampule charged with a stir bar and toluene (25 mL) were added [3,5-$CF_3N^cC^cN]H_3$ (4) (250 mg, 0.425 mmol), and $Mo(NMe_2)_4$ (350 mg, 1.275 mmol). After heating to 40 °C for 4 d all volatiles were removed *in vacuo*. The remaining purple solid was gently heated *in vacuo* to 50 °C for 48 h to sublime the unreacted $Mo(NMe_2)_4$. $^1$H NMR (300 MHz, $C_6D_6$, δ): 7.34 (br. s, 1H, *ipso*-Ar H), 7.14 (br. s, 2H, Ar H), 7.11 (br. s, 2H, Ar H), 7.05 (br. s, 2H, Ar H), 7.03 (br. s, 1H, Ar H), 7.01 (br. s, 1H, Ar H), 3.73 (t, *J* = 8.35 Hz, 4H, N-C*H*$_2$-), 3.08 (br. s, 36H, N(C*H*$_3$)$_2$), 2.84 (t, *J* = 7.76 Hz, 4H, Ar-C*H*$_2$-). $^{13}$C{$^1$H} NMR (67.57 Hz, $C_6D_6$ 128.39, δ): 37.58 (s, -*C*H$_2$-Ar), 50.50 (s, N(*C*H$_3$)$_3$), 56.52 (s, N-*C*H$_2$-), 110.91 (s, aromatic),

116.48 (s, aromatic), 126.91 (s, aromatic), 127.33 (s, aromatic), 129.59 (s, aromatic), 129.76 (s, aromatic), 132.88 (q, $J$ = 32.06 Hz, $CF_3$), 140.82 (s, aromatic), 156.39 (s, aromatic).

**Synthesis of [$\mu$–(3,5–$CF_3N^CC^CN$]HMg(THF)$_2$ (10)**

MeMgCl (1.30 mL, 3.0 M, 3.9 mmol) in THF (2 mL) was added dropwise to [3,5-$CF_3$-$N^cC^cN$]$H_3$ (**4**) (1.0g, 1.70 mmol) in THF (2 mL) with a magnetic stirbar at -35 °C. After 3 h volatiles were removed *in vacuo* and a dark yellow powder remained. Pentanes (3 mL) were added to the powder and stirred for 12 h. The suspension was filtered and white needle crystals were grown from a concentrated solution of the filtrate at -35 °C over a period of 48 h. Enough product was produced for x-ray analysis and $^1$H NMR but not for EA or $^{13}C\{^1H\}$ NMR spectroscopy. $^1$H NMR (300 MHz, Tol-$D_8$, -75 °C δ): 7.25 (s, 2H, Ar H), 7.16 (s, 2H, Ar H), 7.13 (s, 1H, Ar H), 6.91 (s, 2H, Ar H), 6.77 (t, $J$ = 6.74 Hz, 1H, Ar H), 6.55 (br. s, 2H, Ar H), 3.62 (d, $J$ = 12.31 Hz, 1H, O-C$H_2$-), 3.23 (br. s, 1H, O-C$H_2$-), 3.07 (br. s, 2H, O-C$H_2$-), 2.95 (br. s, 4H, N-C$H_2$-), 2.28 (br. s, 2H, O-C$H_2$-), 2.14 (m (9), 2H, O-C$H_2$-), 0.98 (br. s, 8H, -C$H_2$-C$H_2$-), 0.92 (t, $J$ = 7.33 Hz, 4H, Ar-C$H_2$-).

**Synthesis of [3,5–$CF_3N^CC^CN$]H(SiMe$_3$)$_2$ (11)**

To a solution of THF (2 mL) containing **4** (1.01 g, 1.72 mmol) and a stirbar, MeMgCl (1.3 mL 3 M, 3.25 mmol) in THF (2 mL) was added dropwise at -35 °C. The solution was stirred at ambient temperature for 3 h. Chlorotrimethylsilane (610 mg, 5.65 mmol) of was added at -35 °C. The solution was kept at -35 °C for 1 h then stirred at ambient temperature for 15 h. 1,4-dioxane (2 mL) was then added causing precipitation of $MgCl_2$. The solution was filtered and volatiles were removed *in vacuo* causing crystallization of the product. Yield 931 mg (1.27 mmol, 73.8%). $^1$H NMR (300 MHz, $C_6D_6$, δ): 7.40 (s, 2H, Ar H), 7.35 (s, 4H, Ar H), 7.02 (t, $J$ = 7.61 Hz, 1H, Ar H), 6.77 (dd, $J$ = 1.64, 7.61 Hz, 2H, Ar H), 6.68 (s, 1H, Ar H), 3.23 (t, $J$ = 7.46

Hz, 4H, N-C$H_2$-), 2.48 (t, $J$ = 7.31 Hz, 4H, Ar-C$H_2$-), 0.00 (s, 18H (15H observed), $SiMe_3$). $^{13}C\{^1H\}$ NMR (128.39 $C_6D_6$, δ): 0.74 (s, $Si(CH_3)_3$), 35.60 (s, -$CH_2$-Ar), 49.00 (s, -$CH_2$-N), 112.34 (s, aromatic), 118.74 (s, aromatic), 120.81 (s, aromatic), 122.90(s, aromatic), 129.57 (s, aromatic), 129.57 (s, aromatic), 129.91 (s, aromatic), 132.75 (q, $J$ = 32.23 Hz, $CF_3$), 140.07 (s, aromatic), 150.75 (s, aromatic). $^{19}F\{^1H\}$ NMR ($C_6D_6$, δ): -63.32 (s, $CF_3$). Anal. Calcd for $C_{32}H_{36}F_{12}N_2Si_2$: C, 52.45; H, 4.95; N, 3.82. Found: C, 52.470; H,4.816; N,3.689.

**X–ray Experimental Details For [3,5-$CF_3$-$N^CC^CN$]$H_3$ (4)**

Data were collected at 173 K on a Siemens SMART PLATFORM equipped with A CCD area detector and a graphite monochromator utilizing $MoK_\alpha$ radiation (λ = 0.71073 Å). Cell parameters were refined using up to 8192 reflections. A full sphere of data (1850 frames) was collected using the ω-scan method (0.3° frame width). The first 50 frames were re-measured at the end of data collection to monitor instrument and crystal stability (maximum correction on I was < 1 %). Absorption corrections by integration were applied based on measured indexed crystal faces.

The structure was solved by the Direct Methods in *SHELXTL6*, and refined using full-matrix least squares. The non-H atoms were treated anisotropically, whereas the hydrogen atoms were calculated in ideal positions and were riding on their respective carbon atoms. The asymmetric unit consists of two chemically equivalent but crystallographically independent. They differ by the orientations of the side aryl rings with respect to the central one. Out of the eight $CF_3$ groups, six of them are disordered and were refined in two parts each. A total of 890 parameters were refined in the final cycle of refinement using 10886 reflections with $I > 2\sigma(I)$ to yield $R_1$ and $wR_2$ of 6.33% and 13.87%, respectively. Refinement was done using $F^2$.

**X-ray Experimental Details For $\mu$–(2,6–$^{i}$PrNCN)[Zr(NMe$_2$)$_3$]$_2$ (6)**

Data were collected at 173 K on a Siemens SMART PLATFORM equipped with A CCD area detector and a graphite monochromator utilizing MoK$_\alpha$ radiation ($\lambda$ = 0.71073 Å). Cell parameters were refined using up to 8192 reflections. A full sphere of data (1850 frames) was collected using the ω-scan method (0.3° frame width). The first 50 frames were re-measured at the end of data collection to monitor instrument and crystal stability (maximum correction on I was < 1 %). Absorption corrections by integration were applied based on measured indexed crystal faces.

The structure was solved by the Direct Methods in *SHELXTL6*, and refined using full-matrix least squares. The non-H atoms were treated anisotropically, whereas the hydrogen atoms were calculated in ideal positions and were riding on their respective carbon atoms. A total of 507 parameters were refined in the final cycle of refinement using 10924 reflections with I > 2σ(I) to yield $R_1$ and $wR_2$ of 3.95% and 8.19%, respectively. Refinement was done using $F^2$.

**X–ray Experimental Details For [μ-(3,5–CF3NCCCN)Zr(NMe2)3HNMe2]2 (7)**

Data were collected at 173 K on a Siemens SMART PLATFORM equipped with A CCD area detector and a graphite monochromator utilizing MoK$_\alpha$ radiation ($\lambda$ = 0.71073 Å). Cell parameters were refined using up to 8192 reflections. A full sphere of data (1850 frames) was collected using the ω-scan method (0.3° frame width). The first 50 frames were re-measured at the end of data collection to monitor instrument and crystal stability (maximum correction on I was < 1 %). Absorption corrections by integration were applied based on measured indexed crystal faces.

The structure was solved by the Direct Methods in *SHELXTL6*, and refined using full-matrix least squares. The non-H atoms were treated anisotropically, whereas the hydrogen atoms

were calculated in ideal positions and were riding on their respective carbon atoms. The asymmetric unit consists of a half dimer and a benzene solvent molecule. The complex had all four CF3 groups disordered and each set of three F atoms was refined in three positions with their site occupation factors dependently refined to a total of on1. All F atoms were refined with isotropic displacement parameters. A total of 543 parameters were refined in the final cycle of refinement using 7414 reflections with $I > 2\sigma(I)$ to yield $R_1$ and $wR_2$ of 5.37% and 13.33%, respectively. Refinement was done using $F^2$.

The toluene molecule were disordered and could not be modeled properly, thus program SQUEEZE, a part of the PLATON package of crystallographic software, was used to calculate the solvent disorder area and remove its contribution to the overall intensity data.

**X–ray Experimental Details for [$\mu$–(3,5–$CF_3N^CC^CN$]HMg(THF)$_2$ (10)**

Data were collected at 173 K on a Siemens SMART PLATFORM equipped with A CCD area detector and a graphite monochromator utilizing $MoK_\alpha$ radiation ($\lambda$ = 0.71073 Å). Cell parameters were refined using up to 8192 reflections. A full sphere of data (1850 frames) was collected using the $\omega$-scan method (0.3° frame width). The first 50 frames were re-measured at the end of data collection to monitor instrument and crystal stability (maximum correction on I was < 1 %). Absorption corrections by integration were applied based on measured indexed crystal faces.

The structure was solved by the Direct Methods in *SHELXTL6*, and refined using full-matrix least squares. The non-H atoms were treated anisotropically, whereas the hydrogen atoms were calculated in ideal positions and were riding on their respective carbon atoms. Two of the four CF3 groups are disordered one in two part and the other in three parts. Their site occupation factors were dependently refined and their displacement parameters were treated isotropically. A

total of 556 parameters were refined in the final cycle of refinement using 4126 reflections with I > 2σ(I) to yield $R_1$ and $wR_2$ of 5.60% and 14.61%, respectively. Refinement was done using $F^2$.

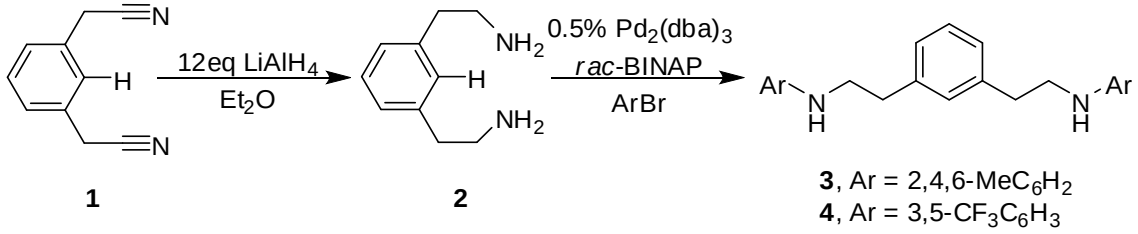


Scheme 2-1. Synthesis of $ArN^{C}C^{C}NH_3$ (where Ar = 2,4,6-$MeC_6H_3$ (**3**) and 3,5–$CF_3C_6H_3$ (**4**)).

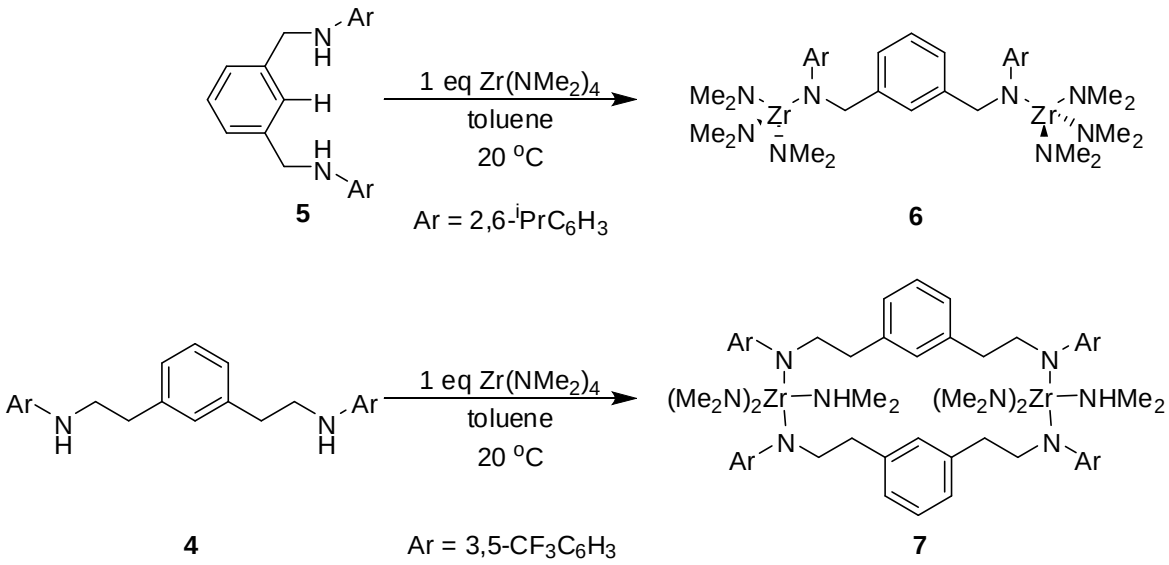


Scheme 2-2. Synthesis of **6** and **7** (where Ar = 2,4-$^{i}PrC_6H_3$ (**6**) and 3,5–$CF_3C_6H_3$ (**7**)).

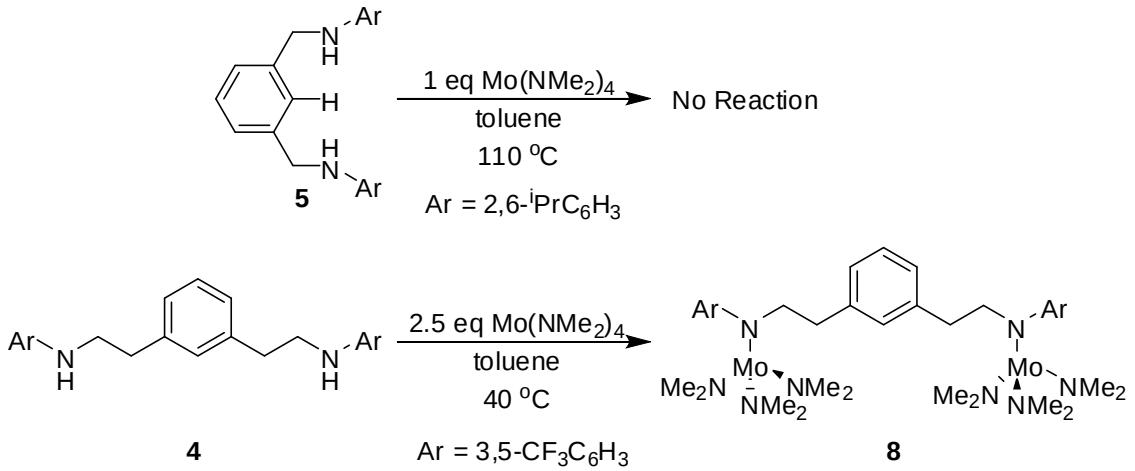


Scheme 2-3. Dramatic reactivity difference between ligands **4** and **5**. Synthesis of the molybdenum dinuclear species $\mu$–(3,5–$CF_3N^CC^CN$)[$Mo(NMe_2)_3$]$_2$ (**8**).

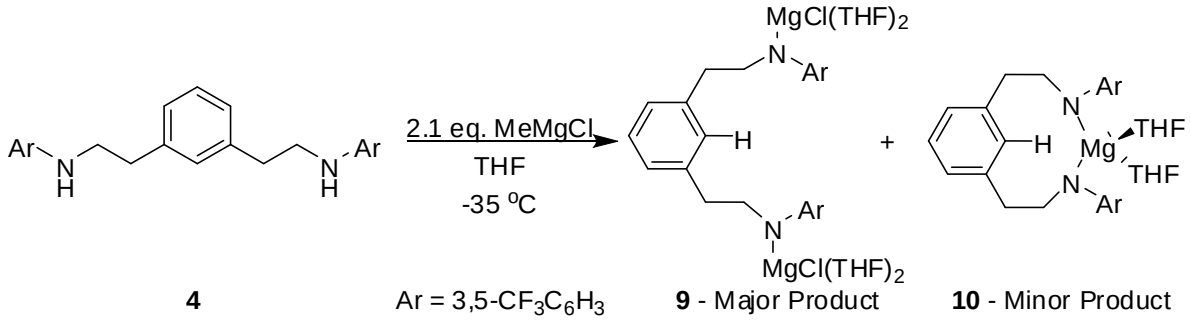


Scheme 2-4. Synthesis of the dimagnesio salt [3,5–$CF_3N^CC^CN$]H[$MgCl(THF)_2$]$_2$ (**9**) and the minor impurity monomagnesio salt [$\mu$–(3,5–$CF_3N^CC^CN$]$HMg(THF)_2$ (**10**).

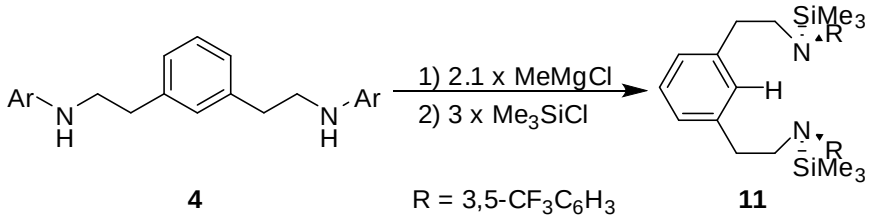


Scheme 2-5. Synthesis of the bistrimethylsilyl species [3,5–$CF_3N^CC^CN$]H($SiMe_3$)$_2$ (**11**).

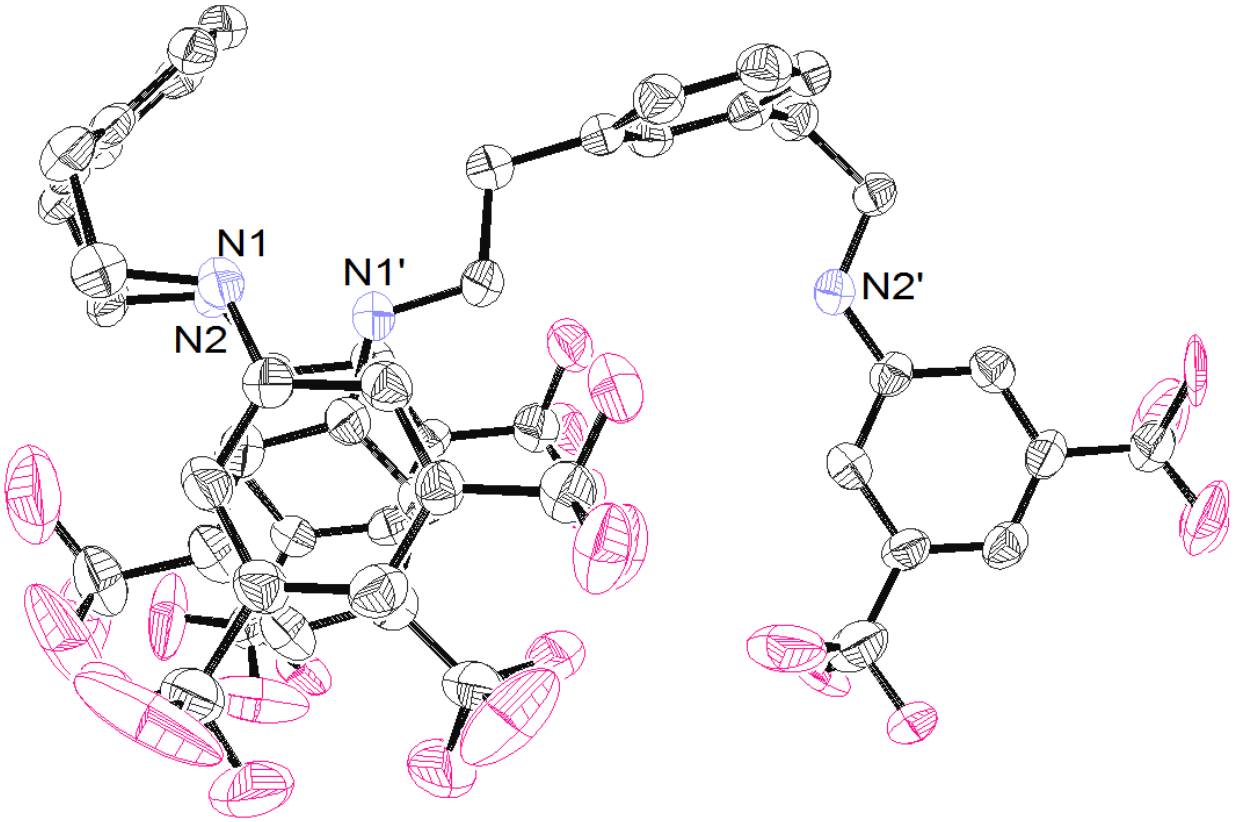


Figure 2-1. ORTEP diagram of [3,5–$CF_3N^CC^CN]H_3$ (**4**). Thermal ellipsoids are displayed at the 50% probability level. Hydrogen atoms and cocrystallized solvent molecules are omitted for clarity.

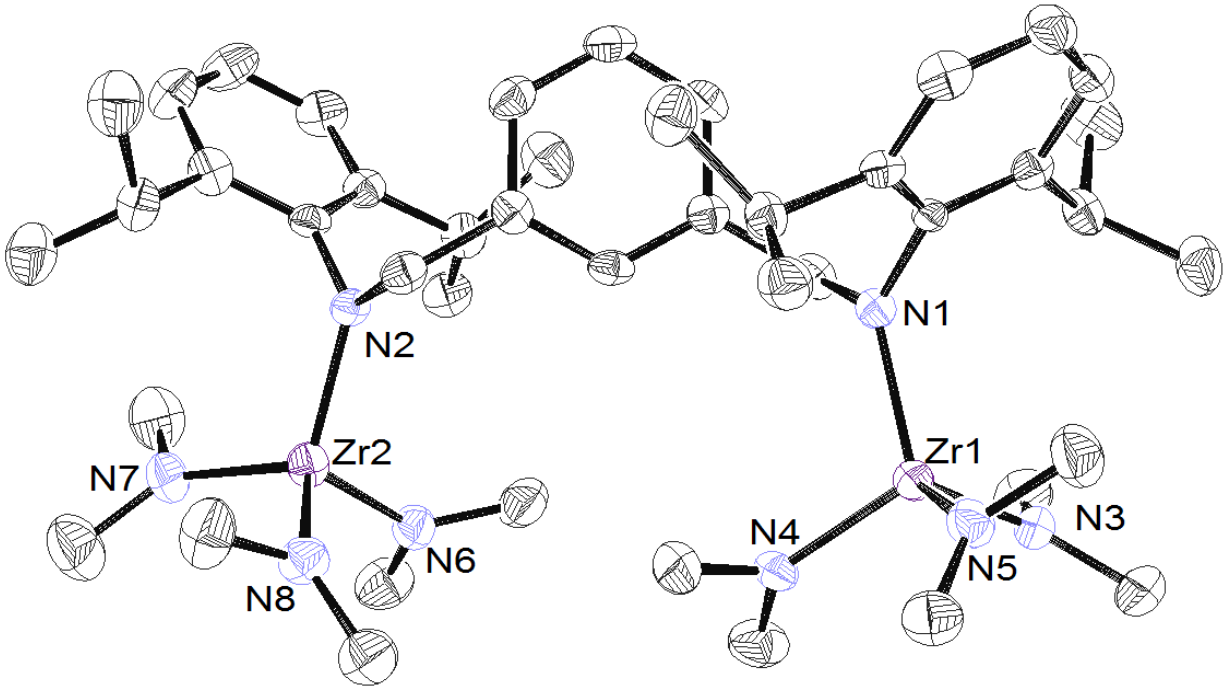


Figure 2-2. ORTEP diagram of (2,6-$^{i}$Pr-NCN)[Zr($NMe_2$)$_3$]$_2$ (**6**). Thermal ellipsoids are displayed at the 50% probability level. Hydrogen atoms and cocrystallized solvent molecules are omitted for clarity.

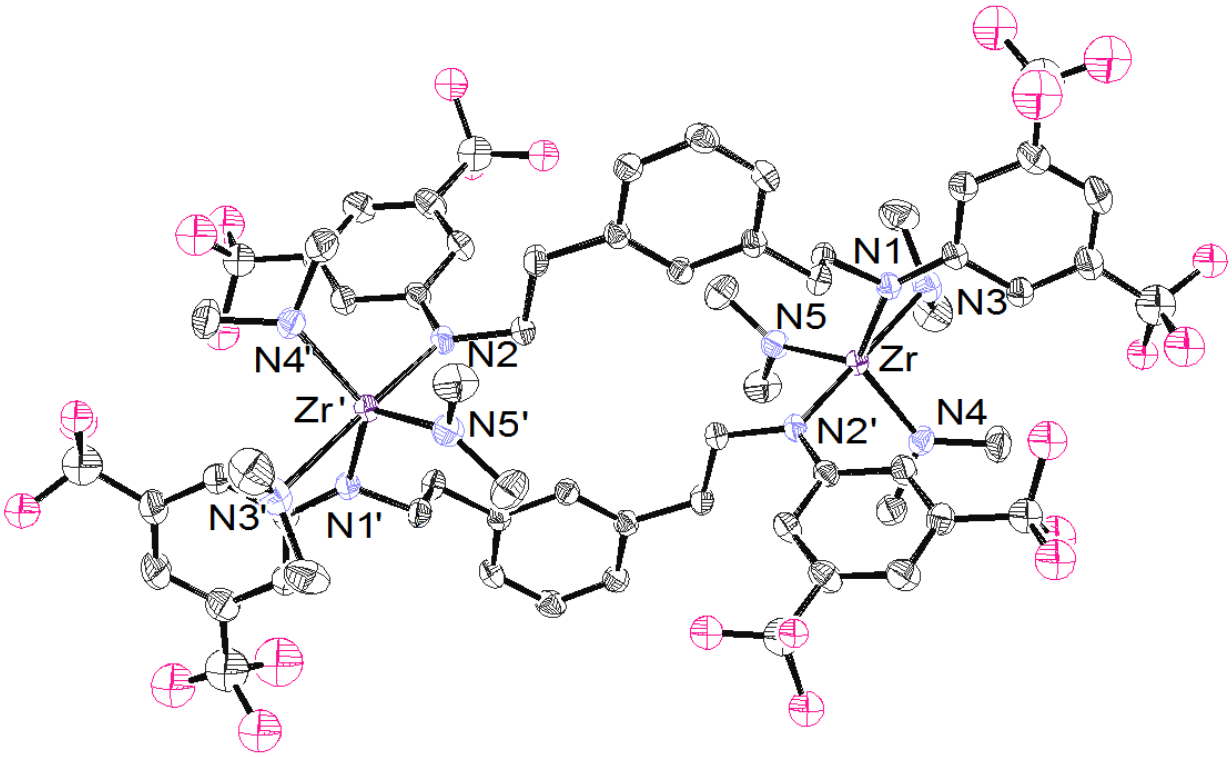


Figure 2-3. ORTEP diagram of $\mu$-(3,5–$CF_3$-$N^CC^CN$)[$Zr(NMe_2)_2(HNMe_2)]_2$ (**7**). Thermal ellipsoids are displayed at the 50% probability level. Hydrogen atoms and cocrystallized solvent molecules are omitted for clarity.

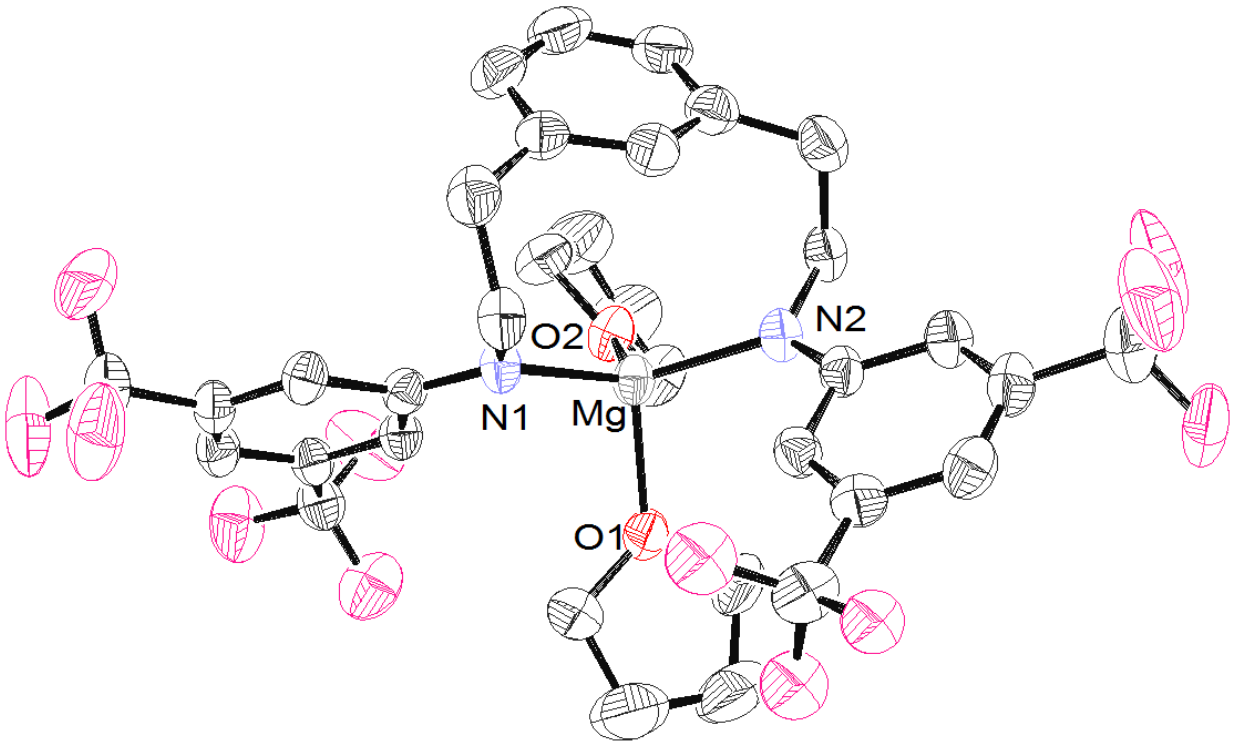


Figure 2-4. ORTEP diagram of [$\mu$–(3,5–$CF_3N^CC^CN$]$HMg(THF)_2$ (**10**). Thermal ellipsoids are displayed at the 50% probability level. Hydrogen atoms and cocrystallized solvent molecules are omitted for clarity.

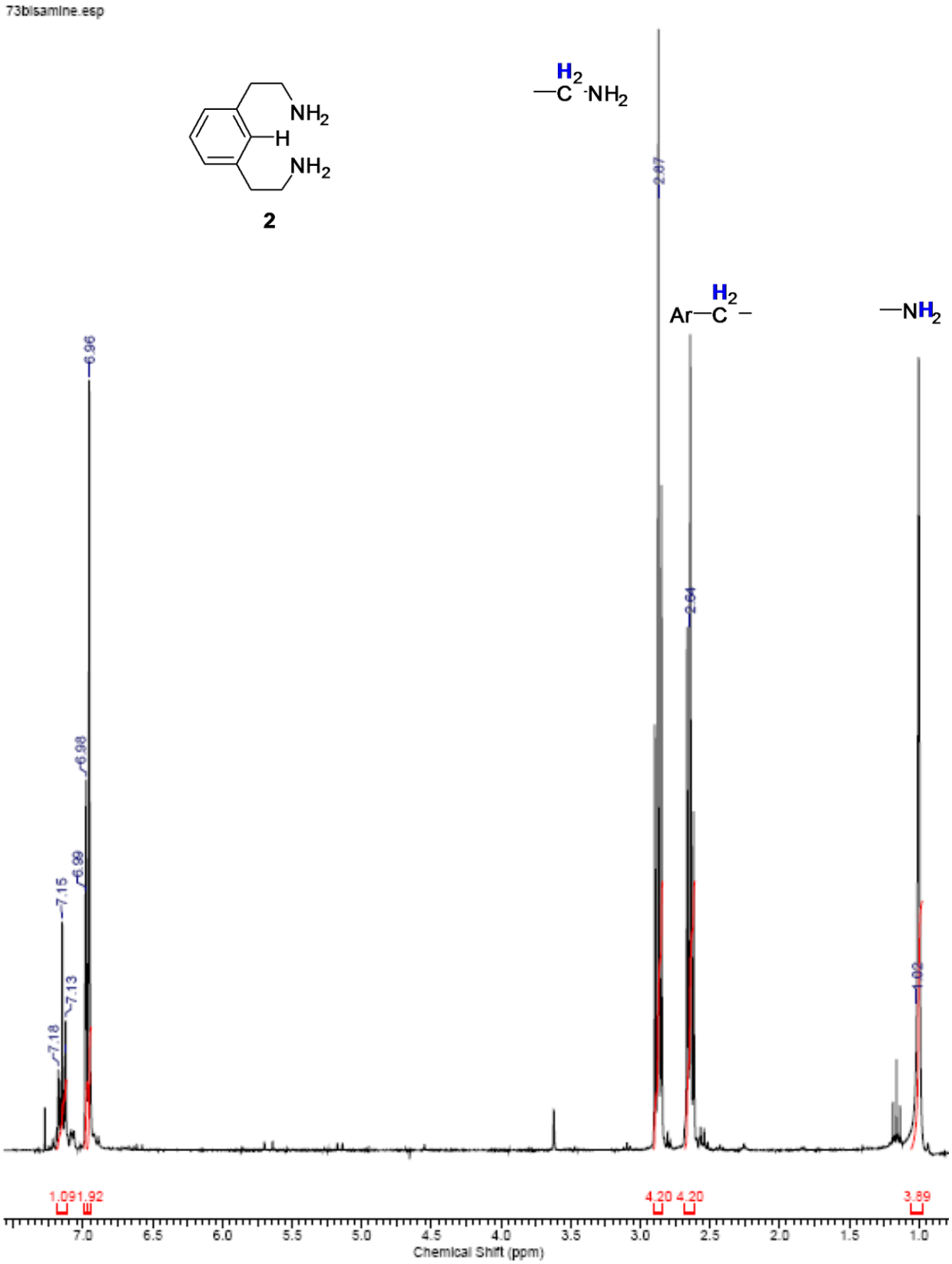


Figure 2-5. $^{1}$H NMR spectra of 2,2'-(1,3-phenylene)diethanamine (**2**) in $C_6D_6$.

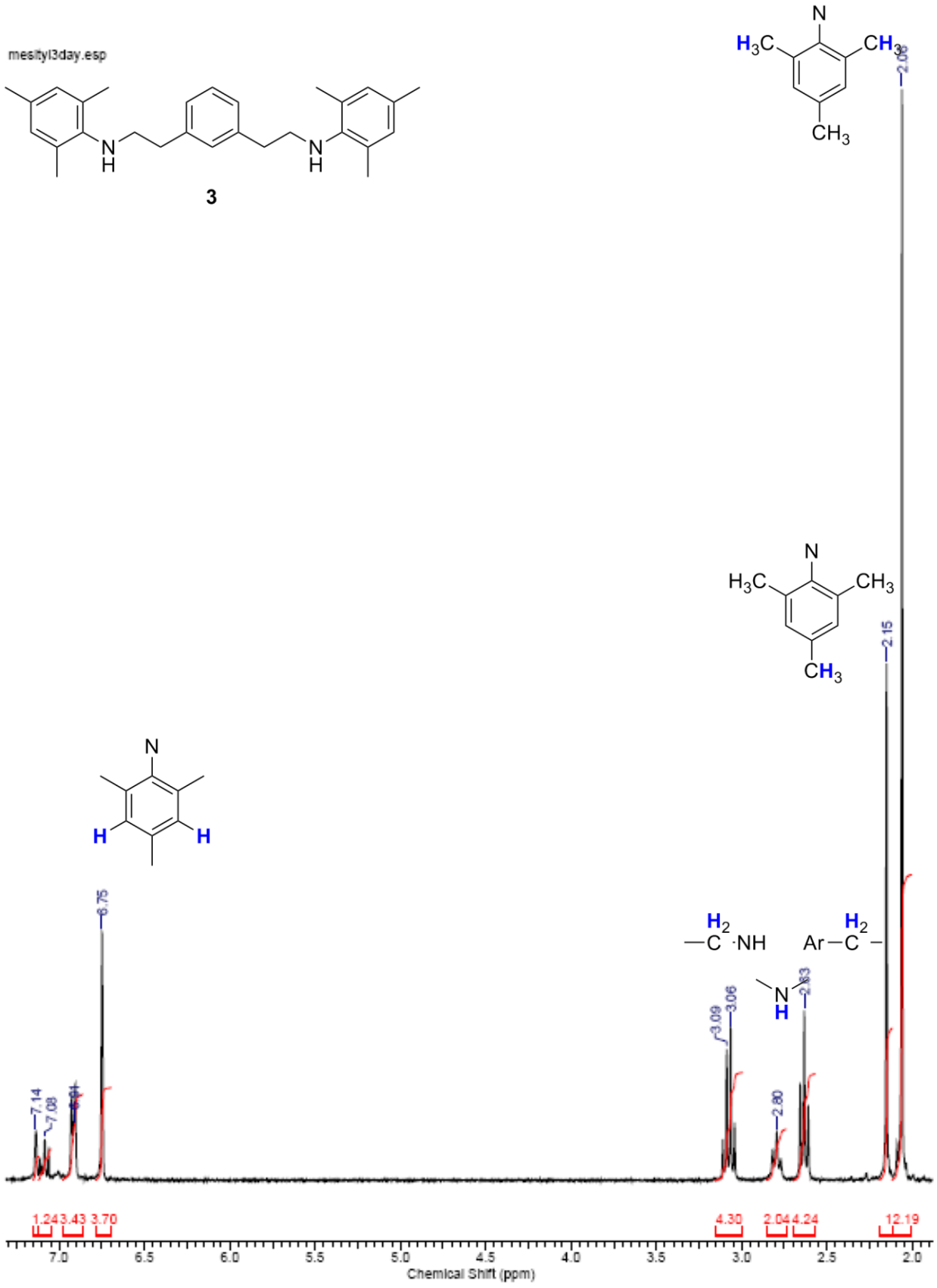


Figure 2-6. $^{1}H$ NMR spectra of [2,4,6-Me$N^{C}C^{C}N$]$H_3$ (**3**) in $C_6D_6$.

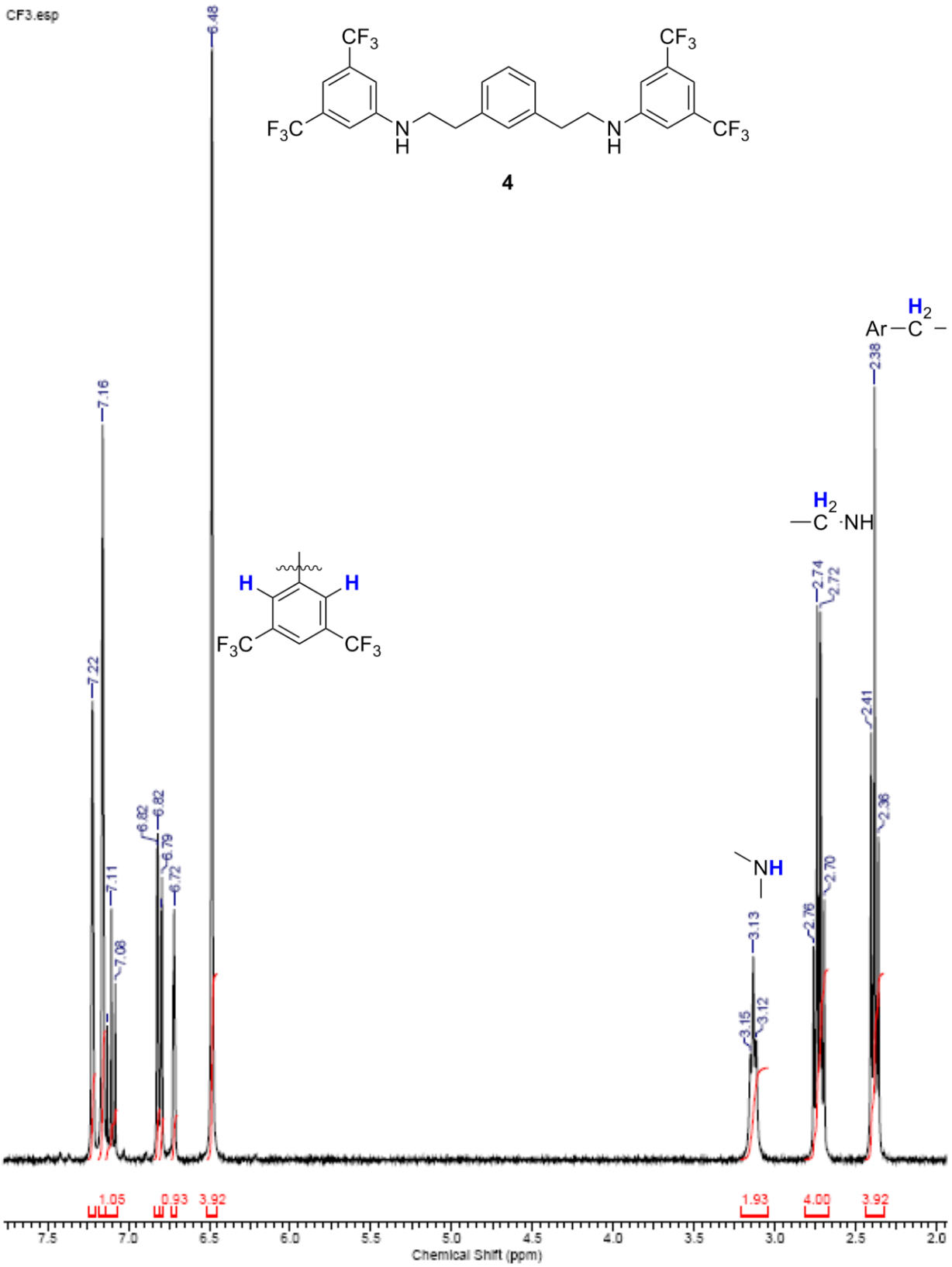


Figure 2-7. $^{1}$H NMR spectra of [3,5-$CF_3N^CC^CN]H_3$ (**4**) in $C_6D_6$.

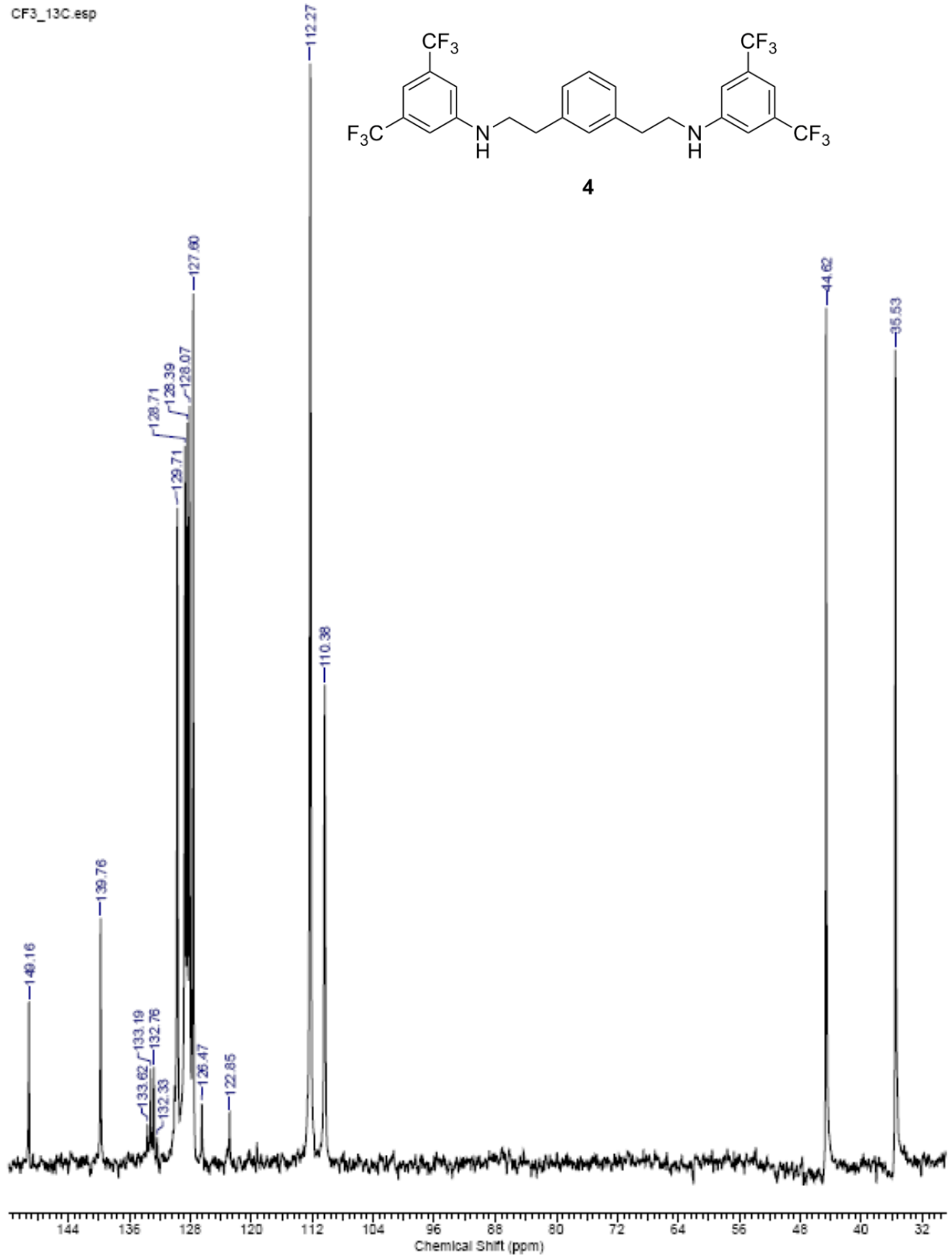


Figure 2-8. $^{13}C\{^{1}H\}$ NMR spectrum of $[3,5\text{-}CF_3N^CC^CN]H_3$ (**4**) in $C_6D_6$.

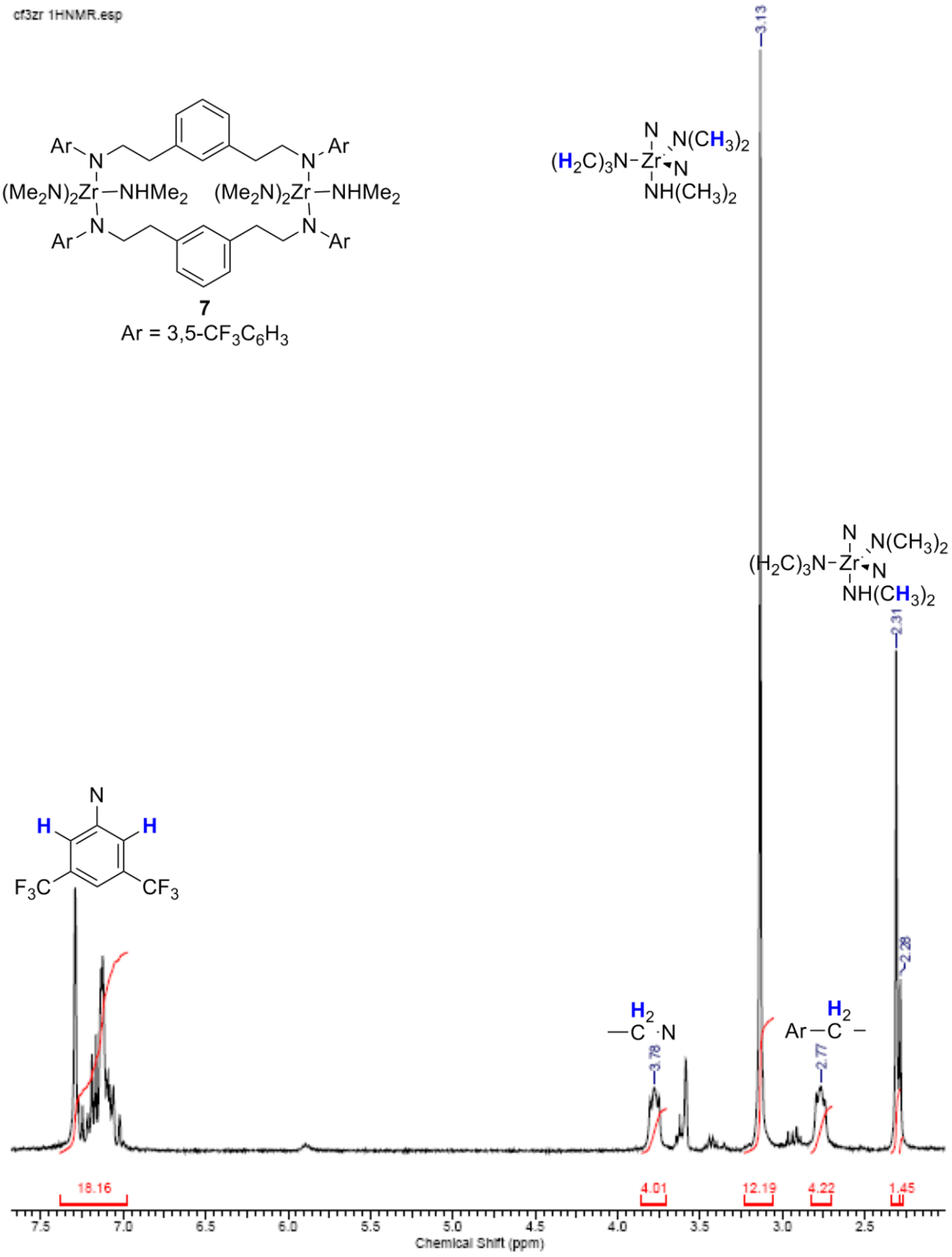


Figure 2-9. $^{1}$H NMR spectra of [$\mu$-(3,5–$CF_3N^CC^CN$)Zr($NMe_2$)$_3$H$NMe_2$]$_2$ (**7**) in $C_6D_6$.

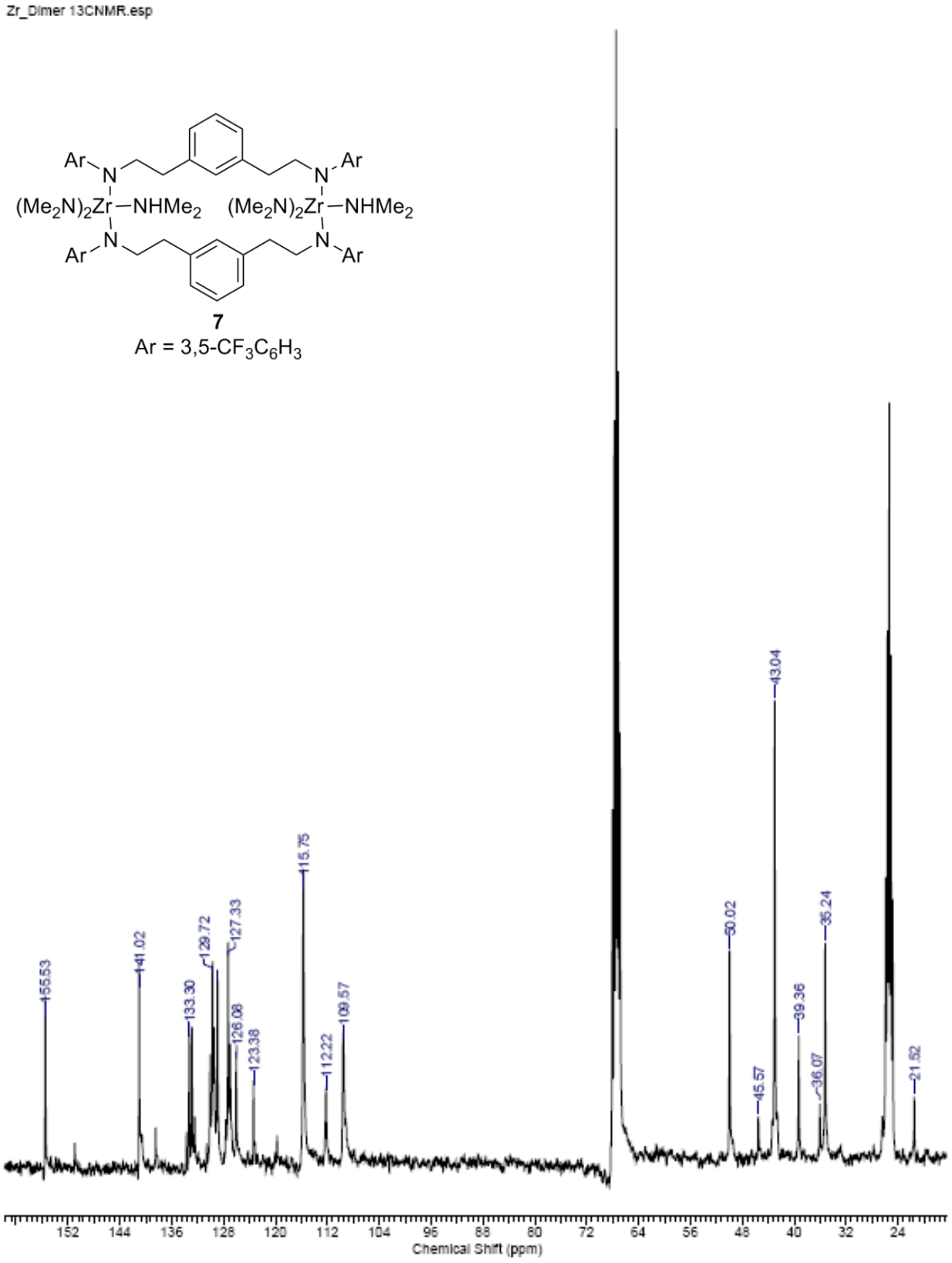


Figure 2-10. $^{13}C\{^{1}H\}$ NMR spectrum of [$\mu$-(3,5–$CF_3N^CC^CN$)$Zr(NMe_2)_3HNMe_2]_2$ (**7**) in THF-$d_8$.

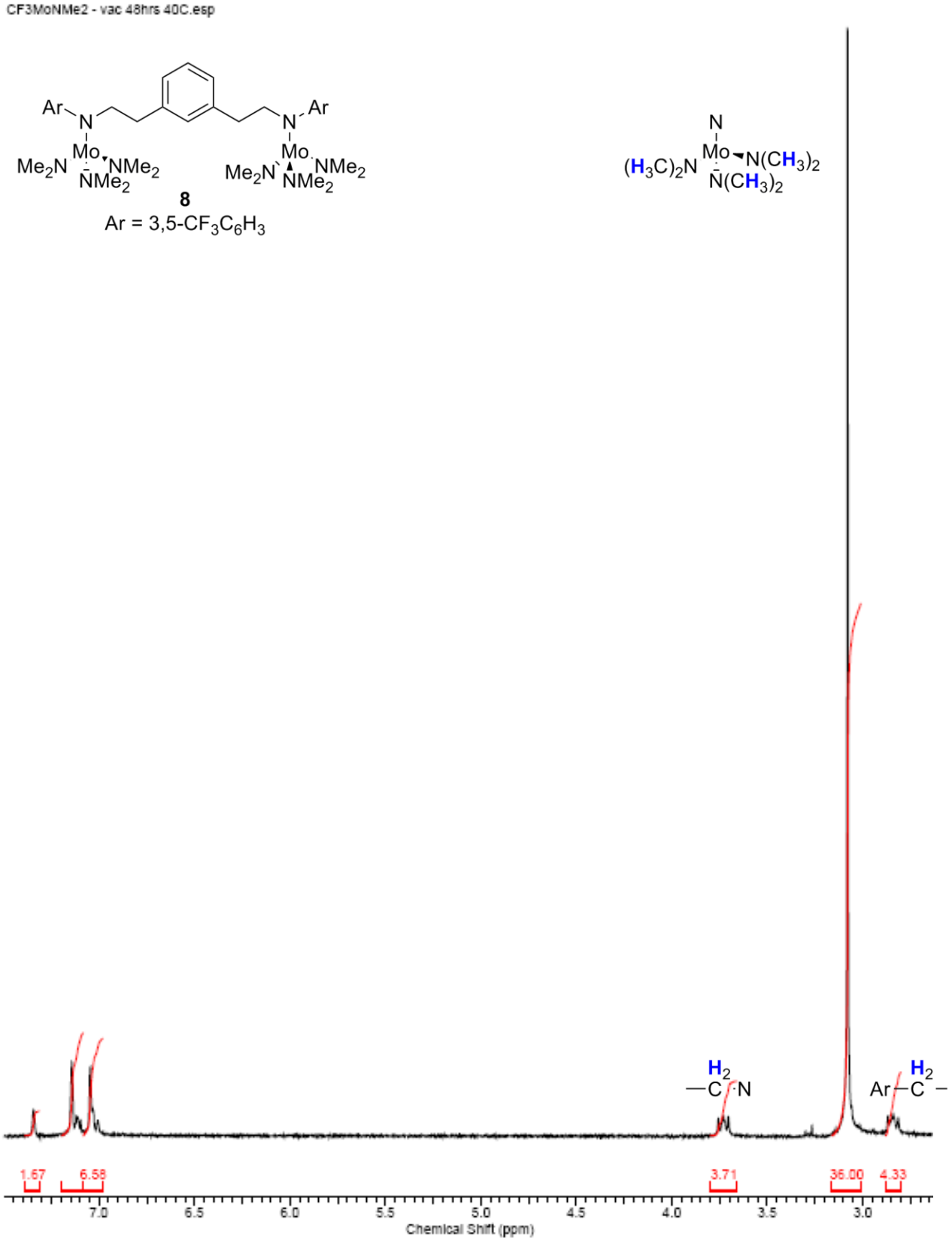


Figure 2-11. $^{1}$H NMR spectra of $\mu$–(3,5–$CF_3N^CC^CN$)[$Mo(NMe_2)_3]_2$ (**8**) in $C_6D_6$.

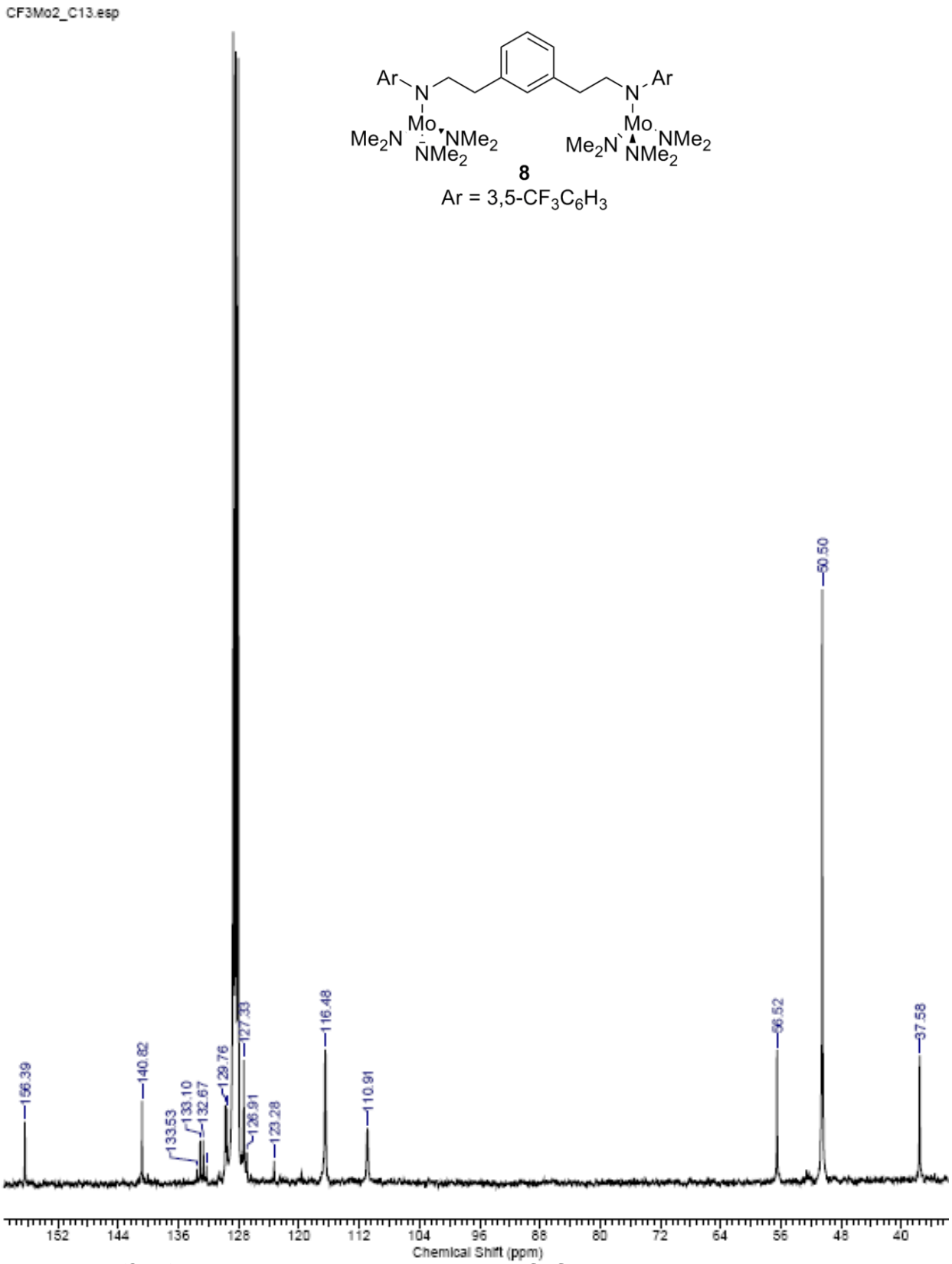


Figure 2-12. $^{13}C\{^{1}H\}$ NMR spectrum of $\mu$–(3,5–$CF_3N^CC^CN$)[$Mo(NMe_2)_3]_2$ (**8**) in $C_6D_6$.

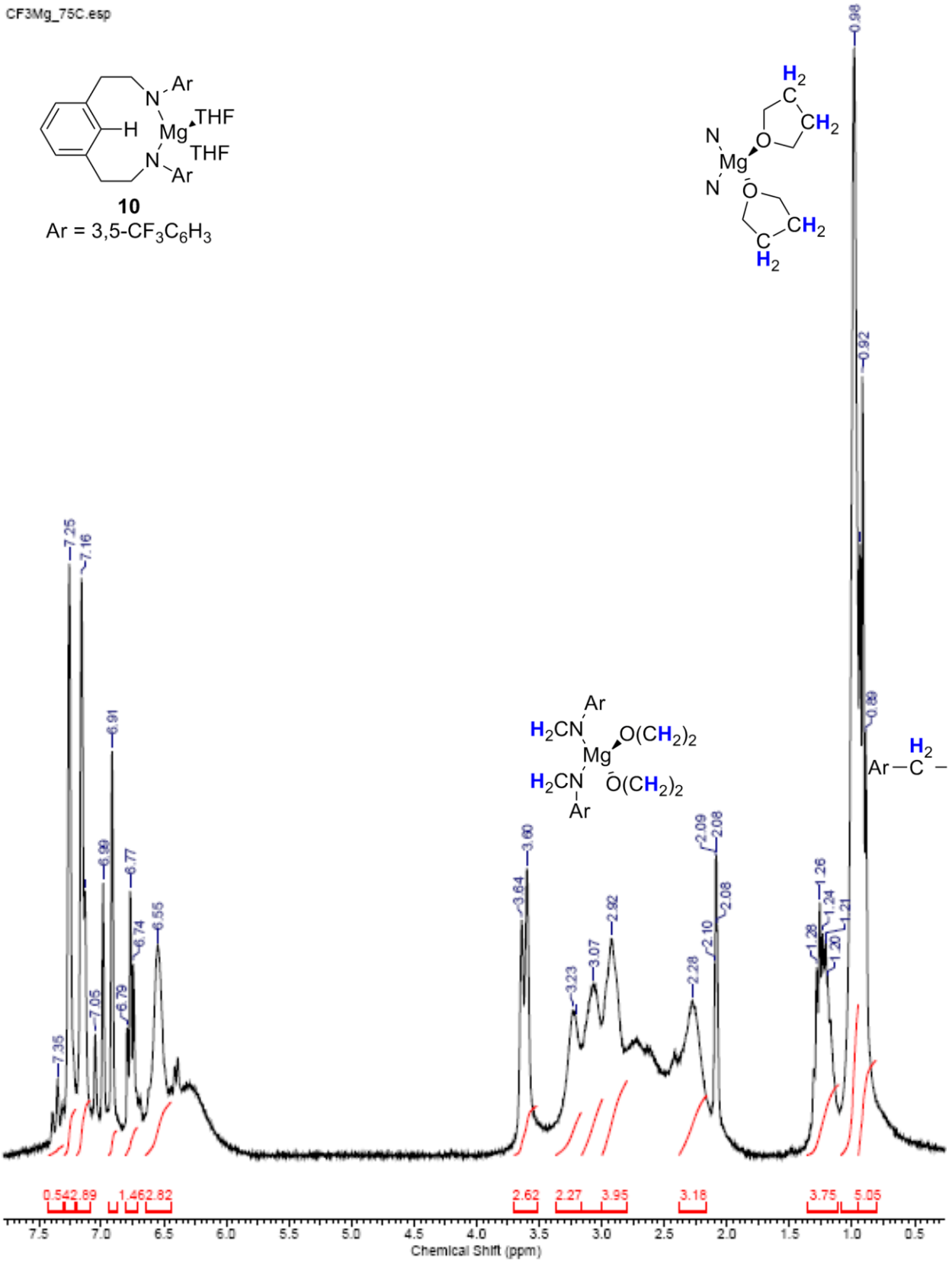


Figure 2-13. $^{1}$H NMR spectra of [3,5-$CF_3N^CC^CN$]HMg(THF)$_2$ (**10**) in Tol-$d_8$ @ -75 °C.

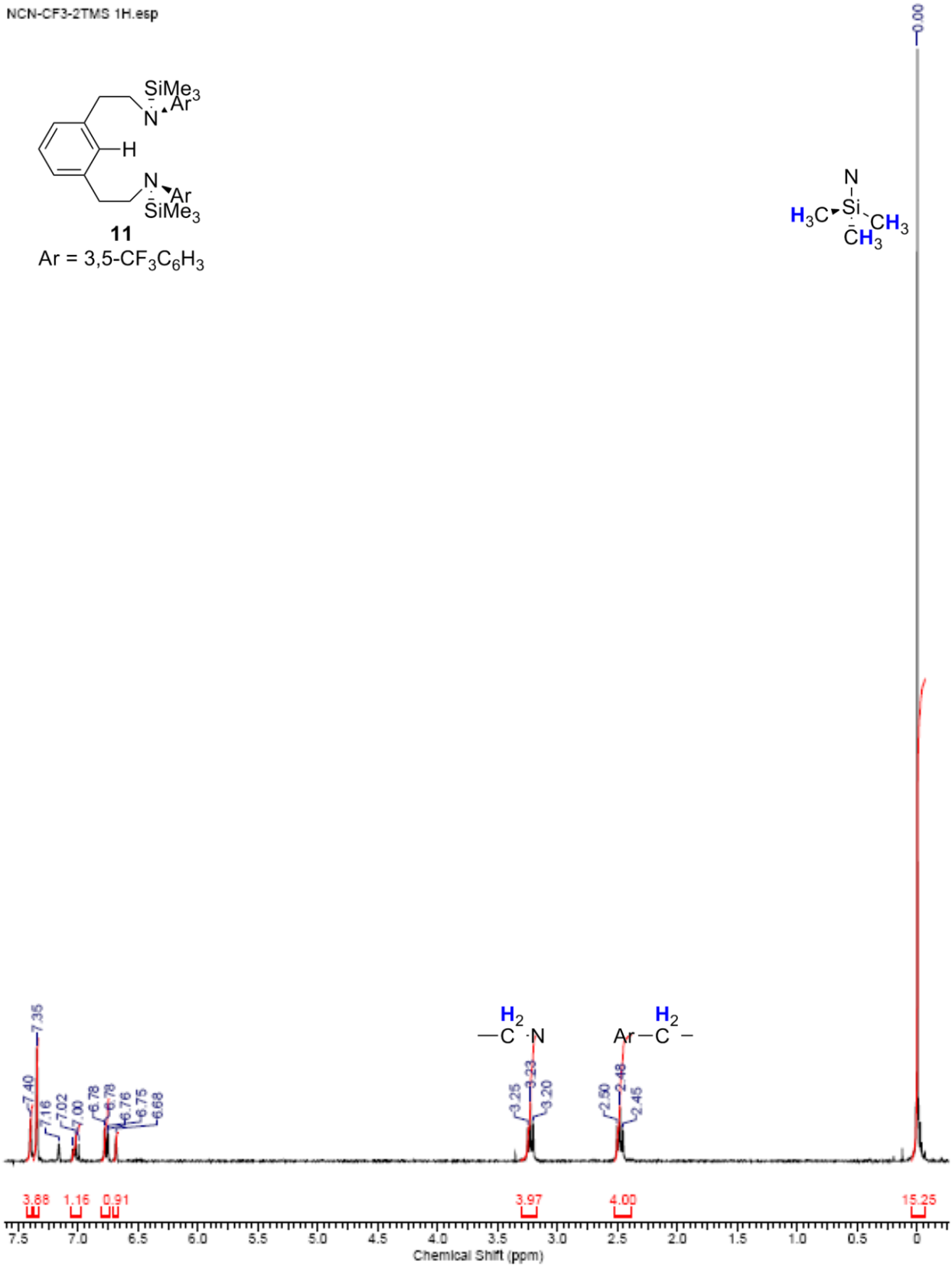


Figure 2-14. $^{1}$H NMR spectra of [3,5–$CF_3N^CC^CN$]H($SiMe_3$)$_2$ (**11**) in $C_6D_6$.

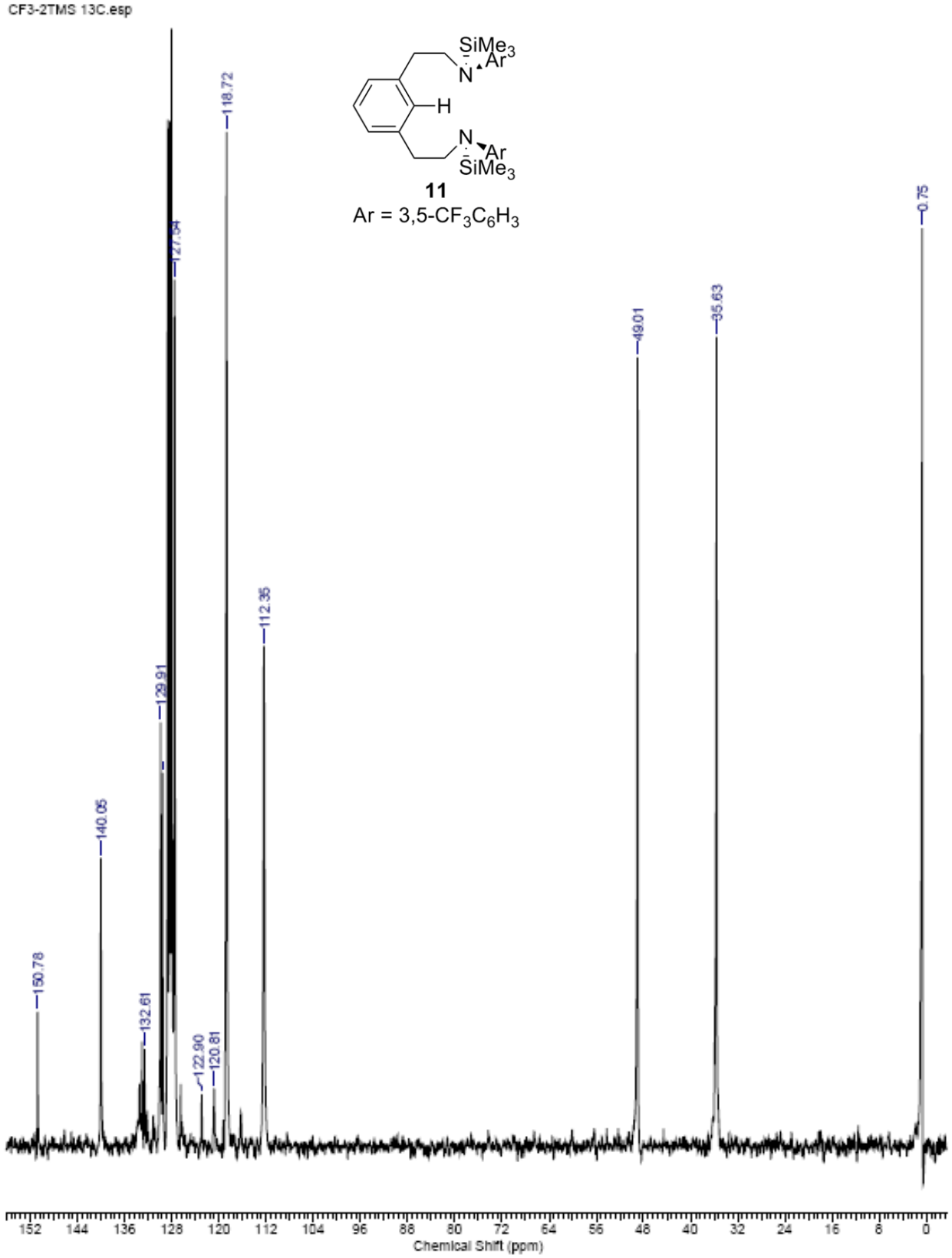


Figure 2-15. $^{13}C\{^{1}H\}$ NMR spectrum of [3,5–$CF_3N^CC^CN$]H($SiMe_3$)$_2$ (**11**) in $C_6D_6$.

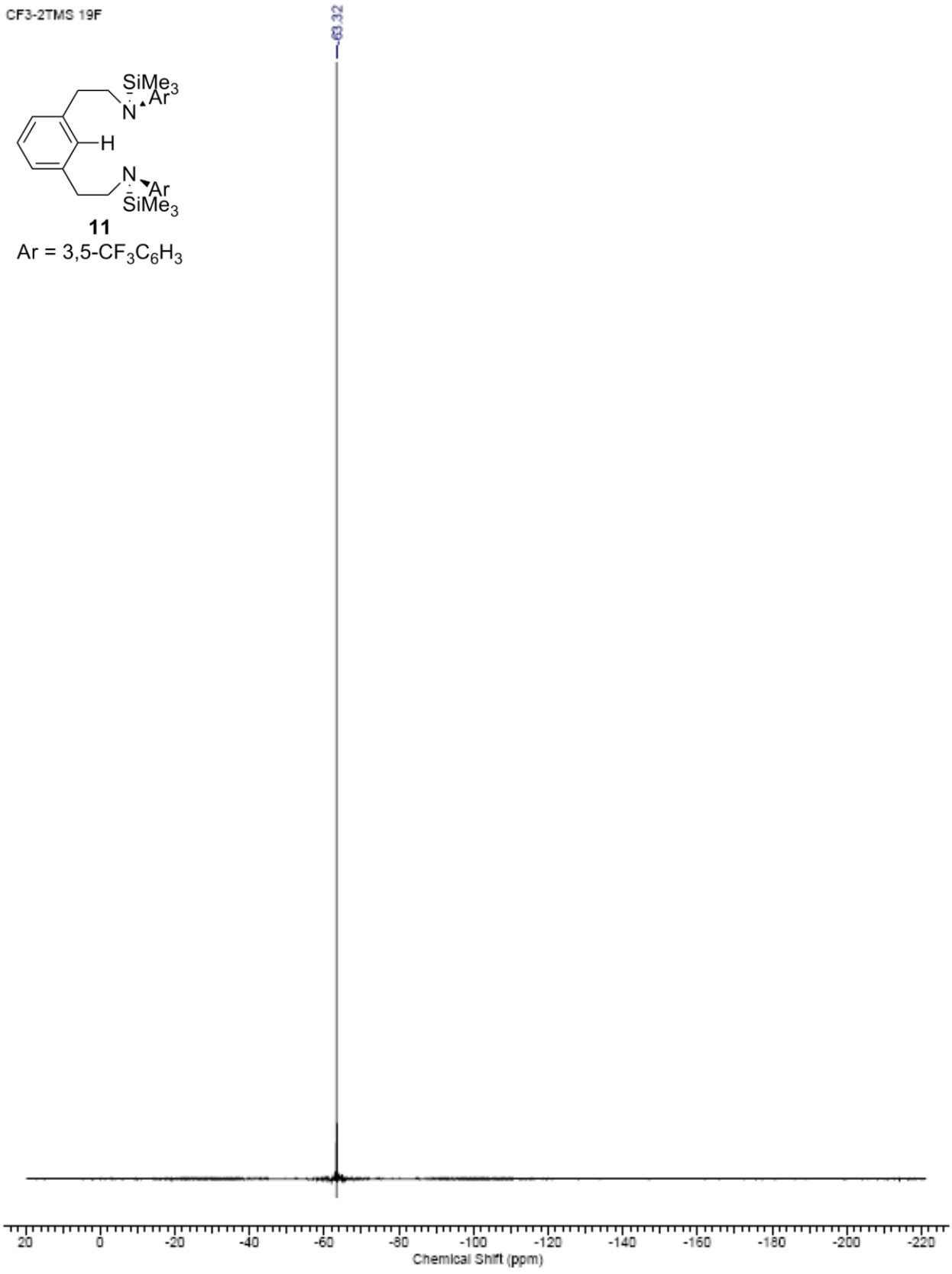


Figure 2-16. $^{19}F$ NMR spectrum of [3,5–$CF_3N^CC^CN$]H$(SiMe_3)_2$ (**11**) in $C_6D_6$.

Table 2-1. Selected angles and bond lengths for crystal structures **6**, **7**, and **10**

| (2,6-$^{i}$Pr-NCN)[Zr(NMe$_2$)$_3$]$_2$ (**6**) | | $\mu$-(3,5–CF$_3$-N$^{C}$C$^{C}$N)[Zr(NMe$_2$)$_2$(HNMe$_2$)]$_2$ (**7**) | | [$\mu$–(3,5–CF$_3$N$^{C}$C$^{C}$N]HMg(THF)$_2$ (**10**) | |
|---|---|---|---|---|---|
| Bond Lengths (Å) | | | | | |
| Zr-N1 | 2.137(2) | Zr-N4 | 2.036(3) | Mg-O2 | 2.0140(18) |
| Zr-N2 | 2.212(2) | Zr-N5 | 2.037(3) | Mg-N1 | 2.019(2) |
| Zr-N4 | 2.036(3) | Zr-N1 | 2.137(2) | Mg-N2 | 2.026(2) |
| Zr-N5 | 2.037(3) | Zr-N2 | 2.212(2) | Mg-O1 | 2.0491(18) |
| Zr-N3 | 2.461(3) | Zr-N3 | 2.461(3) | | |
| Zr-N6 | 2.046(3) | | | | |
| Zr-N7 | 2.030(3) | | | | |
| Zr-N8 | 2.034(3) | | | | |
| Bond Angles (deg) | | | | | |
| N4-Zr1-N5 | 110.96(10) | N4-Zr-N5 | 114.44(11) | O2-Mg-N1 | 110.69(8) |
| N4-Zr1-N3 | 105.44(10) | N4-Zr-N1 | 122.10(10) | O2-Mg-N2 | 103.98(8) |
| N5-Zr1-N3 | 107.72(11) | N5-Zr-N1 | 121.45(10) | N1-Mg-N2 | 130.58(9) |
| N4-Zr1-N1 | 108.41(10) | N4-Zr-N2’ | 96.60(10) | O2-Mg-O1 | 100.77(8) |
| N5-Zr1-N1 | 114.12(10) | N5-Zr-N2’ | 95.28(10) | N1-Mg-O1 | 103.00(8) |
| N3-Zr1-N1 | 109.82(10) | N1-Zr-N2’ | 92.44(9) | N2-Mg-O1 | 103.86(8) |
| N7-Zr2-N8 | 108.84(11) | N4-Zr-N3 | 85.90(11) | | |
| N7-Zr2-N6 | 105.30(11) | N5-Zr-N3 | 88.61(11) | | |
| N8-Zr2-N6 | 108.31(11) | N1-Zr-N3 | 81.62(10) | | |
| N7-Zr2-N2 | 114.06(10) | N2-Zr-N3’ | 174.00(10) | | |
| N8-Zr2-N2 | 108.74(10) | | | | |
| N6-Zr2-N2 | 111.40(10) | | | | |

Table 2-2. Crystal data, structure solution and refinement for [3,5–$CF_3N^CC^CN]H_3$ (**4**)

| | |
|---|---|
| identification code | (ac04) |
| empirical formula | $C_{26}H_{20}F_{12}N_2$ |
| formula weight | 588.44 |
| $T$ (K) | 173(2) |
| $\lambda$ (Å) | 0.71073 |
| crystal system | Triclinic |
| space group | P-1 |
| $a$ (Å) | 11.9159(14) |
| $b$ (Å) | 14.003(2) |
| $c$ (Å) | 16.6156(18) |
| $\alpha$ (deg) | 75.343(2) |
| $\beta$ (deg) | 71.727(2) |
| $\gamma$ (deg) | 74.212(2) |
| $V$ (Å$^3$) | 2490.3(5) |
| Z | 4 |
| $\rho_{calcd}$ (Mg mm$^{-3}$) | 1.570 |
| abs coeff (mm$^{-1}$) | 0.156 |
| $F$(000) | 1192 |
| crystal size (mm$^3$) | 0.11 x 0.08 x 0.05 |
| $\theta$ range for data collection | 1.31 to 22.50 |
| limiting indices | -11≤h≤12, -15≤k≤13, -12≤l≤17 |
| no. of reflns collcd | 10886 |
| no. of ind reflns ($R_{int}$) | 6488 [R(int) = 0.1286] |
| completeness to $\theta$ = 22.50° | 99.8 % |
| absorption corr | Integration |
| refinement method | Full-matrix least-squares on $F^2$ |
| data / restraints / parameters | 6488 / 0 / 890 |
| GOF[c] on $F^2$ | 0.896 |
| $R1$,[a] $wR2$[b] [I > 2σ] | 0.0633, 0.1387 [3149] |
| $R1$,[a] $wR2$[b] (all data) | 0.1350, 0.1701 |
| largest diff. peak and hole | 0.310 and -0.263 e.Å$^{-3}$ |

R1 = $\sum(||F_o| - |F_c||) / \sum|F_o|$, wR2 = $[\sum[w(F_o^2 - F_c^2)^2] / \sum[w(F_o^2)^2]]^{1/2}$, S = $[\sum[w(F_o^2 - F_c^2)^2] / (n-p)]^{1/2}$ , w= $1/[\sigma^2(F_o^2)+(m*p)^2+n*p]$, p = $[\max(F_o^2,0)+ 2* F_c^2]/3$, m & n are constants.

Table 2-3. Crystal data and structure refinement for $\mu$–(2,6–$^{i}$PrNCN)[Zr(NMe$_2$)$_3$]$_2$ (**6**)

| | |
|---|---|
| identification code | (kv13) |
| empirical formula | $C_{44}H_{78}N_8Zr_2$ |
| formula weight | 901.58 |
| $T$ (K) | 173(2) |
| $\lambda$ (Å) | 0.71073 |
| crystal system | Monoclinic |
| space group | $P2_1/n$ |
| $a$ (Å) | 9.5540(4) |
| $b$ (Å) | 19.4781(9) |
| $c$ (Å) | 26.2784(12) |
| $\alpha$ (deg) | 90 |
| $\beta$ (deg) | 98.343(1) |
| $\gamma$ (deg) | 90 |
| $V$ (Å$^3$) | 4838.5(4) |
| Z | 4 |
| $\rho_{calcd}$ (Mg mm$^{-3}$) | 1.238 |
| abs coeff (mm$^{-1}$) | 0.467 |
| $F$(000) | 1912 |
| crystal size (mm$^3$) | 0.18 x 0.10 x 0.09 |
| $\theta$ range for data collection | 1.57 to 27.50° |
| limiting indices | -6≤h≤12, -24≤k≤24, -34≤l≤33 |
| no. of reflns collcd | 30297 |
| no. of ind reflns ($R_{int}$) | 10924 [R(int) = 0.0661] |
| completeness to $\theta$ = 22.50° | 98.3 % |
| absorption corr | Integration |
| refinement method | Full-matrix least-squares on $F^2$ |
| data / restraints / parameters | 10924 / 0 / 507 |
| GOF[c] on $F^2$ | 0.854 |
| $R1$,[a] $wR2$[b] [I > 2σ] | 0.0395, 0.0819 [5881] |
| $R1$,[a] $wR2$[b] (all data) | 0.0884, 0.0879 |
| largest diff. peak and hole | 0.593 and -0.778 e.Å$^{-3}$ |

$R1 = \sum(||F_o| - |F_c||) / \sum|F_o|$ , $wR2 = [\sum[w(F_o^2 - F_c^2)^2] / \sum[w(F_o^2)^2]]^{1/2}$ , $S = [\sum[w(F_o^2 - F_c^2)^2] / (n-p)]^{1/2}$ , $w = 1/[\sigma^2(F_o^2)+(m*p)^2+n*p]$, $p = [\max(F_o^2,0)+ 2* F_c^2]/3$, m & n are constants.

Table 2-4. Crystal data and structure refinement for [$\mu$-(3,5–$CF_3N^CC^CN$)$Zr(NMe_2)_3HNMe_2]_2$ (**7**)

| | |
|---|---|
| identification code | (ac03) |
| empirical formula | $C_{76}$ $H_{86}$ $F_{24}$ $N_{10}$ $Zr_2$ |
| formula weight | 1777.99 |
| $T$ (K) | 173(2) |
| $\lambda$ (Å) | 0.71073 |
| crystal system | Triclinic |
| space group | P-1 |
| $a$ (Å) | 9.1226(5) |
| $b$ (Å) | 12.3882(7) |
| $c$ (Å) | 18.5955(10) |
| $\alpha$ (deg) | 77.615(1) |
| $\beta$ (deg) | 79.183(1) |
| $\gamma$ (deg) | 88.269(1) |
| $V$ (Å$^3$) | 2016.04(19) |
| Z | 1 |
| $\rho_{calcd}$ (Mg mm$^{-3}$) | 1.464 |
| abs coeff (mm$^{-1}$) | 0.362 |
| $F$(000) | 908 |
| crystal size (mm$^3$) | 0.19 x 0.19 x 0.06 |
| $\theta$ range for data collection | 1.68 to 27.50° |
| limiting indices | $-11\leq h\leq 11$, $-15\leq k\leq 15$, $-24\leq l\leq 18$ |
| no. of reflns collcd | 13079 |
| no. of ind reflns ($R_{int}$) | 8784 [R(int) = 0.0386] |
| completeness to $\theta$ = 22.50° | 94.9 % |
| absorption corr | Integration |
| refinement method | Full-matrix least-squares on $F^2$ |
| data / restraints / parameters | 8784 / 4 / 543 |
| GOF[c] on $F^2$ | 1.048 |
| $R1$,[a] $wR2$[b] [I > 2σ] | 0.0537, 0.1333 [7414] |
| $R1$,[a] $wR2$[b] (all data) | 0.0638, 0.1398 |
| largest diff. peak and hole | 0.902 and -0.778 e.Å$^{-3}$ |

$R1 = \sum(||F_o| - |F_c||) / \sum|F_o|$, $wR2 = [\sum[w(F_o^2 - F_c^2)^2] / \sum[w(F_o^2)^2]]^{1/2}$, $S = [\sum[w(F_o^2 - F_c^2)^2] / (n-p)]^{1/2}$ , $w= 1/[\sigma^2(F_o^2)+(m*p)^2+n*p]$, $p = [\max(F_o^2,0)+ 2* F_c^2]/3$, m & n are constants.

Table 2-5. Crystal data and structure refinement for [$\mu$–(3,5–$CF_3N^CC^CN$]HMg(THF)$_2$ (**10**)

| | |
|---|---|
| identification code | (ac11) |
| empirical formula | $C_{39}H_{46}F_{12}MgN_2O_2$ |
| formula weight | 827.09 |
| $T$ (K) | 173(2) |
| $\lambda$ (Å) | 0.71073 |
| crystal system | Monoclinic |
| space group | $P2_1/c$ |
| $a$ (Å) | 17.9480(12) |
| $b$ (Å) | 9.5720(7) |
| $c$ (Å) | 24.8666(17) |
| $\alpha$ (deg) | 90 |
| $\beta$ (deg) | 110.180(1) |
| $\gamma$ (deg) | 90 |
| $V$ (Å$^3$) | 4009.8(5) |
| Z | 4 |
| $\rho_{calcd}$ (Mg mm$^{-3}$) | 1.370 |
| abs coeff (mm$^{-1}$) | 0.136 |
| $F$(000) | 1720 |
| crystal size (mm$^3$) | 0.19 x 0.15 x 0.08 |
| $\theta$ range for data collection | 1.74 to 27.50° |
| limiting indices | $-23\leq h\leq 20$, $-11\leq k\leq 12$, $-31\leq l\leq 32$ |
| no. of reflns collcd | 26429 |
| no. of ind reflns ($R_{int}$) | 9163 [R(int) = 0.0811] |
| completeness to $\theta$ = 22.50° | 99.4 % |
| absorption corr | Integration |
| refinement method | Full-matrix least-squares on $F^2$ |
| data / restraints / parameters | 9163 / 1 / 556 |
| GOF[c] on $F^2$ | 0.862 |
| $R1$,[a] $wR2$[b] [I > 2σ] | 0.0560, 0.1461 [4126] |
| $R1$,[a] $wR2$[b] (all data) | 0.1284, 0.1636 |
| largest diff. peak and hole | 0.416 and -0.317 e.Å$^{-3}$ |

R1 = $\sum(||F_o| - |F_c||) / \sum|F_o|$, wR2 = $[\sum[w(F_o^2 - F_c^2)^2] / \sum[w(F_o^2)^2]]^{1/2}$, S = $[\sum[w(F_o^2 - F_c^2)^2] / (n-p)]^{1/2}$ , w= $1/[\sigma^2(F_o^2)+(m*p)^2+n*p]$, p = $[\max(F_o^2,0)+ 2* F_c^2]/3$, m & n are constants.

# CHAPTER 3
# SYNTHESIS AND REACTIVITY OF TERPHENYL $OCO^{3-}$ PINCER COMPLEXES

## Synthesis and Characterization of Terphenyl [$^t$BuOCO]$H_3$ (17)

Alkoxides react readily with metal amides, owing to the greater affinity of early transition metals for oxygen than for nitrogen.[35,36] Thus, an $OCO^{3-}$ pincer format (**17**) should effect an increase in reactivity and stability with early transition metals. The alkyl groups must be of sufficient size to prevent metal-metal bonds from forming as well as imparting protection to the active site during reactions.[37] The terphenyl framework also imparts greater rigidity to the pincer backbone over the previous $N^CC^CN$ design.

The synthesis of the terphenyl OCO ligand **17** is a five step sequence (Scheme 3-1) starting with selective *ortho*-bromination of 2-*tert*-butylphenol (**12**) to give bromophenol **13**. Phenol **13** is then masked as its methyl ether, and the Grignard derivative of **14** is generated by treatment with magnesium metal. Dibromoiodide **15** is easily made from 2,6-dibromoaniline via diazotization, and is alkylated with **14**. The bismethyl ether **16** is then deprotected by treatment with boron tribromide. Purification by flash column chromatography affords diol **17** as a white solid in 21% yield from **12** (Scheme 3-1). The identity of **17** was verified by $^1$H NMR, $^{13}$C NMR spectrometry and HRMS. The $^1$H NMR spectrum revealed the expected, singlet from two *tert*-butyl groups that integrate to 18 protons at 1.44 ppm and two OH protons at 7.14 ppm. A $^{13}$C NMR spectrum of **17** shows the 10 signals in the aromatic region with two signals at 35.541 and 30.279 ppm assigned to the carbons of the $^t$Bu groups. The calculated mass for **17** is 374.2240 amu and was experimentally found to be 374.2209 amu, confirming the identity of **17** as the desired terphenyl diol.

### Synthesis and Characterization of [$^t$BuOCO]MoNMe$_2$(HNMe$_2$)$_2$ (18)

Diol **17** was treated with purple Mo(NMe$_2$)$_4$ in pentane at -35 °C (Scheme 3-2). As the reaction warms an orange powder precipitates out of solution in 80% yield. Transparent orange crystals were grown at -35 °C from DME over a period of two days.

The broadened peaks in the $^1$H NMR spectrum are characteristic of a paramagnetic Mo(IV) bearing two unpaired electrons. The $^t$Bu groups are visible as a singlet that is shifted from 1.44 ppm in the free ligand to 2.82 ppm upon coordination to Mo. Singlets at 1.73 and -8.72 ppm are attributed to the pair of methyl groups on the coordinated amide. The methyl protons on the amines appear as singlets at 3.45 and 1.98 ppm, with the NH proton at 3.26 ppm. The ligand contributes 6e$^-$ to the metal and another 6e$^-$ are donated from the amide and two amines. An additional 4e$^-$ occupy π-bonding orbitals from the nitrogen and oxygen lone pairs. Considering the additional 2e$^-$from the metal, **18** is an 18e$^-$ complex. The structure of **18** was determined by single crystal X-ray crystallography and the molecular structure is presented in Figure 3-1. Clearly **17** is bound in a terdendate fashion to molybdenum with a dimethylamine in the position *trans* to the *ipso*–carbon of the backbone, and the remaining axial positions are occupied by coordinated dimethylamine and dimethylamide ligands. As expected with molybdenum alkoxide compounds generated from Mo(NMe$_2$)$_4$, dimethylamine remains in the coordination sphere.[38] The amido and amine ligands are easily distinguished since N1 is trigonal whereas N2 and N3 are pyramidal. In addition the M–N bond lengths are significantly different (Table 3-1). The Mo–NMe$_2$ ligand is twisted away from the N2–Mo–N3 plane by 35° to break the otherwise perfect solid–state $C_s$ symmetry. A space-filling model indicates the twist is due to packing forces that place a DME solvent molecule atop the amido group. Considerable strain is imparted to the pincer backbone and is attributable to congestion caused by the dimethylamine

ligand *trans* to C1. The N–Me groups are nearly parallel to the O1– C1–O2 plane which forces them into the $^{t}$Bu's of the pincer. As a result, the $^{t}$Bu groups are strained, creating 33º and 32º torsion angles between the aryl backbone C2–C7 and C6–C17 connections, respectively, and the central ring is bent up by 30º.

### Synthesis and Characterization of [$^{t}$BuOCO]MoCl (19)

To derivatize the complex such that it would be more amenable to salt metathesis, **18** was treated with 3 equiv of lutidine hydrochloride in pentane.[39] Three equivalents were required due to the insolubility of lutidine hydrochloride in pentane (Scheme 3-3). This reaction results in protonation of the remaining amide and installs a chloride *trans* to the M-C bond. The remaining HCl salts were removed from the resulting red powder by filtration. The $^{1}$H NMR spectrum of **19** revealed broadened resonances indicative of a paramagnetic complex. The $^{t}$Bu protons of the ligand appear at 1.37 ppm and the coordinated dimethyl amine protons have shifted upfield to -2.02 ppm. Complex **19** was crystallized from benzene as single crystals up to 5 mm across, which allowed for the structure to be determined by X-ray crystallography. X-ray structure analysis shows the strain observed in the previous structure **18** is relieved, as the ligand has acquired a 33° twist in the backbone along the Cl1-Mo-C1 axis thus imparting **19** $C_2$ symmetry (Figure 3-2). The octahedral Mo(IV) center is coordinated by the pincer ligand, *trans*–dimethyl amines, and a chloride. The coordinated dimethylamines orient off axis by 57° and are rotated 88º with respect to each other, which, again, can be attributed to sterics. The O1-Mo-O1' angle has decreased slightly from 166.45° in **18** to 165.32° (Table 3-1).

The chemistry of **19** was probed and it was determined that the dimethyl amines on **19** are bound tightly and do not release under vacuum nor substitute with THF, DME or CO, even at

elevated temperatures (80 °C). In addition the complex is stable for short periods when exposed to air.

## Conclusions

Development of new trianionic pincer ligands is two-fold. While new ligand designs need to be explored, successful routes to installing these new ligands on metals need to be developed. Stepwise modifications of our original NCN format led to straightforward metallation of molybdenum using an OCO pincer ligand. While the terdentate behavior of an OCO ligand has now been established with molybdenum, metallation will require modification, possibly to utilize molybdenum chlorides as reagents. Alternative metallation routes will avoid coordinated dimethylamines which have proven difficult to remove and can impede further reactivity. Formation of aryloxide alkali salts[40] and aryl ethers[41] are established and can provide insight into alternative metallation routes with **17**. Our previous work exploring reactivity of early transition metals will also aid in this research. Established synthetic routes to our ligands are easily modified to incorporate new designs quickly as needed. The research presented here will provide a solid foundation for future development of trianionic pincer ligands.

## Experimental

### General Considerations

Unless specified otherwise, all manipulations were performed under an inert atmosphere using standard Schlenk or glovebox techniques. Pentane, hexanes, toluene, diethyl ether, tetrahydrofuran, and 1,2–dimethoxyethane were dried using a GlassContour drying column. $C_6D_6$ and toluene-$d_8$ (Cambridge Isotopes) were dried over sodium–benzophenone ketyl, distilled or vacuum transferred and stored over 4 Å molecular sieves. THF-$d_8$ and acetone-$d_6$ (Cambridge Isotopes) was stored over 4 Å sieves and used without further purification.

NMR spectra were obtained on Gemini (300 MHz), VXR (300 MHz), or Mercury (300 MHz) spectrometers. Chemical shifts are reported in δ (ppm). For $^{1}H$ and $^{13}C$ NMR spectra, the residual protio or carbon solvent peak were referenced as an internal reference. GC/MS spectra were recorded on an Agilent 6210 TOF–MS instrument. C, H, and N elemental analysis were determined by Robertson Microlit Laboratories Inc. and Complete Analysis Laboratories.

**Synthesis of 2-bromo-6-*tert*-butylphenol (13)**

This compound was made according to the procedure Zhang *et al.*[42] Purification was achieved by flash column chromatography (3:1 pentane;$CHCl_3$) to give **13** as a clear colorless oil in 81% yield. $^{1}H$ NMR and $^{13}C$ NMR were consistent with those previously reported.

**Synthesis of 1-bromo-3-*tert*-butyl-2-methoxybenzene (14)**

To a solution of **13** (6.06 g, 26 mmol) in DMF (30mL) was added $K_2CO_3$ (5.5 g, 1.5 equiv., 40 mmol) and MeI (2.5 mL, 1.5 equiv., 40 mmol). The resulting mixture was stirred at ambient temperature for 16 h. Water was added, and the mixture was extracted (2X) with $Et_2O$. The combined organic extracts were washed successively with water, saturated $Na_2S_2O_3$ and brine, dried over $MgSO_4$, filtered and concentrated *in vacuo* to a yellow oil. Methyl ether **14** was obtained by vacuum distillation (58-60 C @ 4 mTorr) as a white crystalline solid (5.76g. 90% yield). $^{1}H$ NMR (300 MHz, DMSO-d6) δ 7.47 (dd, $^{3}J$ = 8.1 Hz, $^{4}J$ = 1.5 Hz, 1H), 7.29 (dd, $^{3}J$ = 8.1 Hz, $^{4}J$= 1.5 Hz, 1H), 6.97 (dd, $J$ = $J$ = 8.1 Hz, 1H), 3.83 (s, OC*H*3, 3H), 1.33 (s, tBu, 9H); $^{13}C$ NMR DMSO-d6) δ 30.6 [C(*C*H3)3], 35.1 [*C*(CH3)], 61.1 (O*C*H3), 117.4 (*C*Br), 125.0 (=H*C*-CH-CBr), 126.6 (tBu-*C*H), 131.9 (=*C*H-CBr), 144.7 (*C*-$^{t}$Bu), 156.1 (*C*OMe); HRMS (GC-E1-C1) calc'd (found) for $C_{11}H_{15}BrO$ ($M^{+}$) 242.0301 (242.0286).

**Synthesis of 1,3-dibromo-2-iodobenzene (15)**

This compound was made according to the procedure of Hart and coworkers.[43] The compound was recrystallized from isopropano before use. $^{1}H$ and $^{13}C$ NMR were consistent with those previously reported.

**Synthesis of 3,3”-di-*tert*-butyl-2,2”-dimethoxy-1,1’:3’,1”-terphenyl (16)**

This compound was made following the general procedure of Hart and coworkers.[43] To a solution of **2** (4.84 g, 3.5 equiv., 20 mmol) in dry THF (40 mL) was added Mg turnings (540 mg, 3.9 equiv., 22 mmol). The resulting mixture was heated to reflux for an additional 1 h. A solution of **3** (2.06 g, 1 equiv., 5.7 mmol) in dry THF (20 mL) was added dropwise over 1 h to the reaction mixture. The resulting mixture was heated at reflux for 16 h. The mixture was cooled to room temperature, and was quenched with 6N HCl. The mixture was extracted with $Et_2O$ (3 x 20 mL). The combined organix extracts were washed with saturated $Na_2S_2O_3$ and brine, dried over $MgSO_4$, filtered and concentrated *in vacuo* to a brown oil. Terphenyl **16** was obtained via flash column chromatography (8:1 hexanes:$CHCl_3$) as a white solid (1.3 g, 57% yield). $^{1}H$ NMR (300 MHz, $C_6D_6$) δ: $^{13}C$ NMR ($C_6D_6$) δ 31.5 [C(CH3)3], 35.7 [C(CH3)3], 60.7 (OCH3), 124.2 (C $^{5,5”}$), 127.0 (C $^{4’,6’}$), 128.4 (C $^{3,3”}$), 129.3 (C $^{2,2”}$), 130.5 (C $^{5’}$), 130.7 (C $^{6,6”}$), 136.1 (C $^{1,1”}$), 141.2 (C $^{1’,3’}$), 143.6 (C $^{3,3”}$), 158.4 (C $^{2,2”}$); HRMS (DIP-C1-MS) calc’d (found) for $C_{28}H_{34}O_2$ ($M^+$) 402.2553 (402.2536).

**Synthesis of 3,3”-di-*tert*-butyl-1,1’:3’,1”-terphenyl-2,2”-diol ([$^{t}$BuOCO]$H_3$) (17)**

To a solution of **16** (1.3 g, 3.2 mmol) in $CH_2Cl_2$ (20 mL) at 0 ºC was added $BBr_3$ (1.6 mL, **5** equiv., 16 mmol). The mixture was warmed slowly to room temperature over 6 h. MeOH was added to quench the reaction, and the mixture was concentrated under reduced pressure. Diol **17** was obtained by flash column chromatography of the residue (5:1 pentane:$CHCl_3$) as a white

solid (600 mg, 50% yield). $^{1}$H NMR (300 MHz, acetone-$d_6$) δ 7.58 (dd, $J$ = $J$ = 7.8 Hz, 1H, $H^{2'}$), 7.54 (dd, $J$ = $J$ = 1.8 Hz, 1H, $H^{5'}$), 7.38 (dd, $^{3}J$ = 7.8 Hz, $^{4}J$ = 1.8 Hz, $H^{4',6'}$), 7.28 (dd, $^{3}J$ = 8.1 Hz, $^{4}J$ = 1.8 Hz, 2H), 7.14 (s, 2 H, OH), 7.07 (dd, $^{3}J$ = 8.1 Hz, $^{4}J$ = 1.8 Hz, 2H), 6.89 (dd, $J$ = $J$ = 8.1 Hz, 2H, $H^{5,5"}$), 1.44 (s, 18H, *t*Bu); $^{13}$C NMR ($C_6D_6$) δ 30.3 [C($CH_3$)$_3$], 35.5 [$C$($CH_3$)$_3$], 121.0 ($C^{5,5"}$), 127.7 ($C^{2'}$), 128.8 ($C^{4',6'}$), 129.0 ($C^{1,1"}$), 129.1 ($C^{4,4"}$), 130.7 ($C^{6,6"}$), 131.5 ($C^{5}$), 137.0 ($C^{1',3'}$), 139.6 ($C^{3,3"}$), 151.7 ($C^{2,2"}$); HRMS (DIP-C1-MS) calc'd (found) for $C_{26}H_{30}O_2$ ($M^+$) 374.2240 (374.2209).

**Synthesis of [$^{t}$BuOCO]MoNMe$_2$(HNMe$_2$)$_2$ (18)**

To a solution of [$^{t}$BuOCO]$H_3$ ligand (**17**) (500 mg, 1.34 mmol) in pentane (2 mL) Mo($NMe_2$)$_4$ (218mg, 1 equiv., 1.34 mmol) in pentane (2 mL) was added quickly at -35 ˚C. The resulting brown slurry was stirred with a spatula until it was warmed to room temperature. The orange precipitate was filtered off, washed with cold pentane and dried *in vacuo*. The product ([3,3"–di–*tert*–butyl–2,2"–di(hydroxy–κO)–1,1':3',1"–terphenyl–2'–yl–κC2'](*N*–methylmethanaminato)bis(*N*–methylmethanamine)molybdenum(IV))) (**18**) was recrystallized from DME as dark orange crystals at -35 ˚C; Yield 642mg (1.07 mmol, 80%) $^{1}$H NMR (300 MHz, THF-$D_8$, δ): 9.61 (br. s, 2H, Ar H), 3.78 (s, 2H, Ar H), 3.45 (br. s, 3H, -NH(C$H_3$)$_2$), 3.26 (s, 1H, -N$H$($CH_3$)$_2$), 3.17 (s, 1H, Ar H), 2.82 (s, 18H, -C(C$H_3$)$_3$), 2.14 (s, 2H, Ar Hs), 1.98 (br. s, 9H, -NH(C$H_3$)$_2$), 1.73 (s, 3H, -N(C$H_3$)$_2$), -8.72 (s, 3H, -N(C$H_3$)$_2$). $^{13}$C{$^{1}$H} NMR (67.57 Hz, THF-$D_8$, δ): 29.76 (s, C, aromatic), 40.55 (s, CH, aromatic), 43.77 (s, -N($C$H3)2), 47.28 (s, CH, aromatic), 49.08 (s, -C($CH_3$)$_3$), 58.31 (s, -$C$($CH_3$)$_3$), 72.02 (s, CH, aromatic), 79.92 (br. s, C, aromatic), 164 (br. s, C-O, aromatic). Anal. Calcd for $C_{32}H_{47}MoN_3O_2$ C, 63.88; H, 7.87; N, 6.98. Found C, 61.13; H, 6.90; N,3.63.

**Synthesis of [$^t$BuOCO]Mo(HNMe$_2$)$_2$Cl (19)**

To a solution of [$^t$BuOCO]Mo(NMe$_2$)(HNMe$_2$)$_2$ (**18**) (250 mg, 0.415 mmol) in pentane (2 mL) was added lutidine HCl (180 mg, 3 equiv., 1.260 mmol). After vigorous stirring for 12 h all volatiles were removed *in vacuo* and the remaining solid was dissolved in THF (2 mL). Remaining lutidine HCl salts were filtered off with a medium porosity fritted funnel. Volatiles from the filtrate were removed *in vacuo* and the remaining solid was triturated with pentane to yield OCO$^t$BuMo(HNMe$_2$)Cl (**19**) as a dark red powder. The product was recrystallized from benzene as dark red crystals; Yield 99 mg (0.167 mmol, 40%) $^1$H NMR (300 MHz, $C_6D_6$, δ): 29.40 (s, 2H, Ar H), 3.57 (br s, 1H, Ar H), 2.42 (s, 2H, Ar H), 1.55 (s, 2H, Ar H), 1.37 (s, 18H, -C-(C*H*$_3$)$_3$), -1.40 (s, 3H, NH-(C*H*$_3$)$_2$), -2.02 (s, 3H, NH-(C*H*$_3$)$_2$), -2.25 (br. s, 9H, -N*H*-(C*H*$_3$)$_2$), -5.32 (s, 2H, Ar Hs). $^{13}$C{$^1$H} NMR (67.57 Hz, THF-D$_8$, δ): 30.20 (s, -NH-(*C*H$_3$)$_2$), 41.24 (s, –C(*C*H$_3$)$_3$), 44.95 (s, -*C*(CH$_3$)$_3$), 128.93 (s, CH, aromatic), 129.08 (s, CH, aromatic), 129.44 (s, CH, aromatic), 163.11 (s, CH, aromatic), 173.11 (s, CH, aromatic). Anal. Calcd for $C_{42}H_{41}D_{12}ClMoN_2O_2$ (2 $C_6D_6$) C, 66.22; H, 6.96; N,3.68. Found: C,66.03; H,7.05; N,3.72.

**X–ray Experimental Details For [$^t$BuOCO]MoNMe$_2$(HNMe$_2$)$_2$ (18)**

Data were collected at 173 K on a Siemens SMART PLATFORM equipped with A CCD area detector and a graphite monochromator utilizing MoK$_\alpha$ radiation (λ = 0.71073 Å). Cell parameters were refined using up to 8192 reflections. A full sphere of data (1850 frames) was collected using the ω-scan method (0.3° frame width). The first 50 frames were re-measured at the end of data collection to monitor instrument and crystal stability (maximum correction on I was < 1 %). Absorption corrections by integration were applied based on measured indexed crystal faces.

The structure was solved by the Direct Methods in *SHELXTL6*, and refined using full-matrix least squares. The non-H atoms were treated anisotropically, whereas the hydrogen atoms were calculated in ideal positions and were riding on their respective carbon atoms. In addition to the complex, there is a dme molecule in the asymmetric unit. The protons, H1 and H2, on N1 and N2 respectively, were obtained from a Difference Fourier map and refined without any constraints. A total of 405 parameters were refined in the final cycle of refinement using 5629 reflections with $I > 2\sigma(I)$ to yield $R_1$ and $wR_2$ of 4.77% and 9.57%, respectively. Refinement was done using $F^2$.

**X–ray Experimental Details For [$^t$BuOCO]Mo(HNMe$_2$)$_2$Cl (19)**

Data were collected at 173 K on a Siemens SMART PLATFORM equipped with A CCD area detector and a graphite monochromator utilizing $MoK_\alpha$ radiation ($\lambda$ = 0.71073 Å). Cell parameters were refined using up to 8192 reflections. A full sphere of data (1850 frames) was collected using the $\omega$-scan method (0.3° frame width). The first 50 frames were re-measured at the end of data collection to monitor instrument and crystal stability (maximum correction on I was < 1 %). Absorption corrections by integration were applied based on measured indexed crystal faces.

The structure was solved by the Direct Methods in *SHELXTL6*, and refined using full-matrix least squares. The non-H atoms were treated anisotropically, whereas the hydrogen atoms were calculated in ideal positions and were riding on their respective carbon atoms. The asymmetric unit consists of a half complex and a benzene molecule of crystallization. The N proton was located in a Difference Fourier map and refined freely. The complexes are located on 2-fold rotation axes of symmetry. A total of 223 parameters were refined in the final cycle of

refinement using 3320 reflections with $I > 2\sigma(I)$ to yield $R_1$ and $wR_2$ of 2.63% and 7.71%, respectively. Refinement was done using $F^2$.

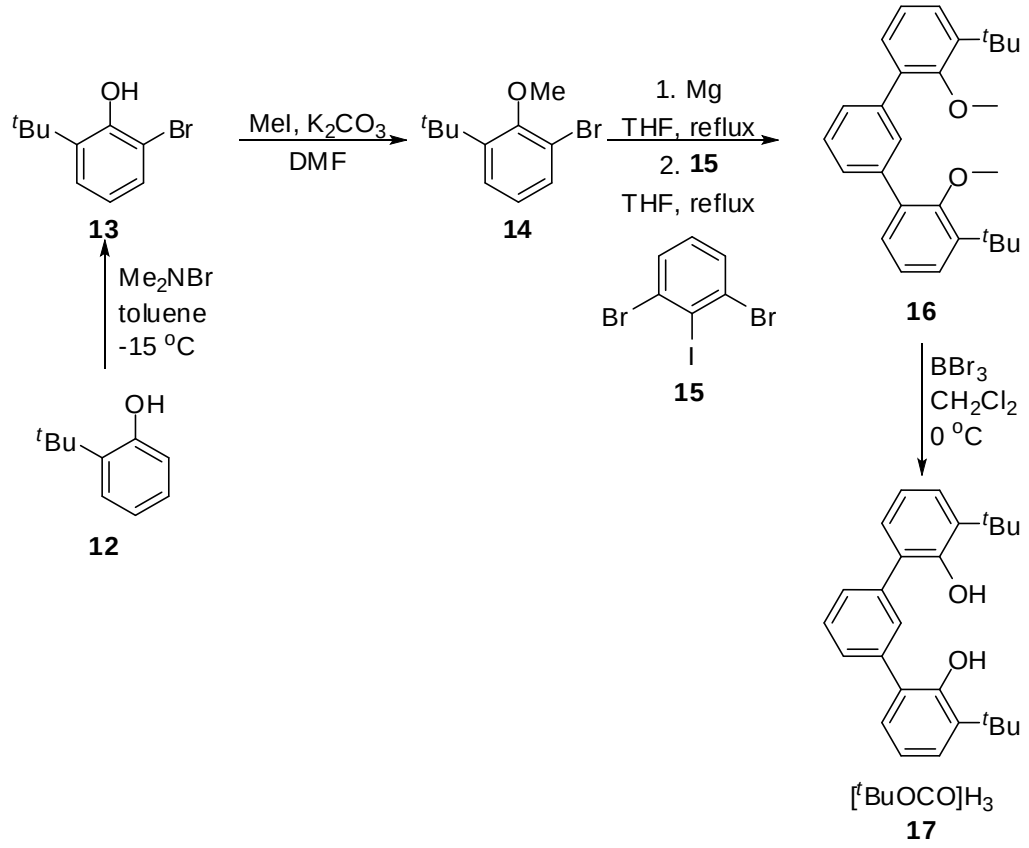


Scheme 3-1. Synthesis of $[^t\text{BuOCO}]H_3$ (**17**).

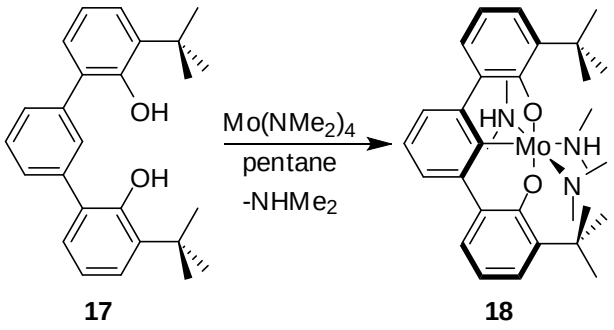


Scheme 3-2. Synthesis of $[^t\text{BuOCO}]\text{MoNMe}_2(\text{HNMe}_2)_2$ (**18**).

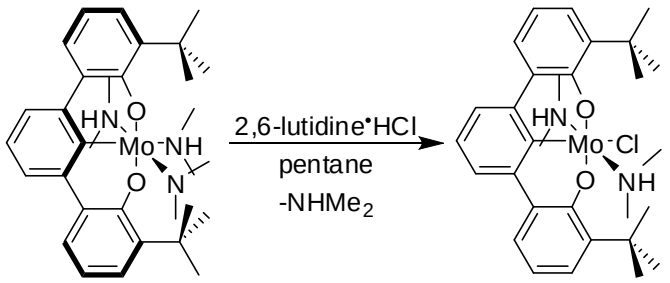


**18** **19**

Scheme 3-3. Synthesis of [$^t$Bu-TP]Mo(HNMe$_2$)$_2$Cl (**19**).

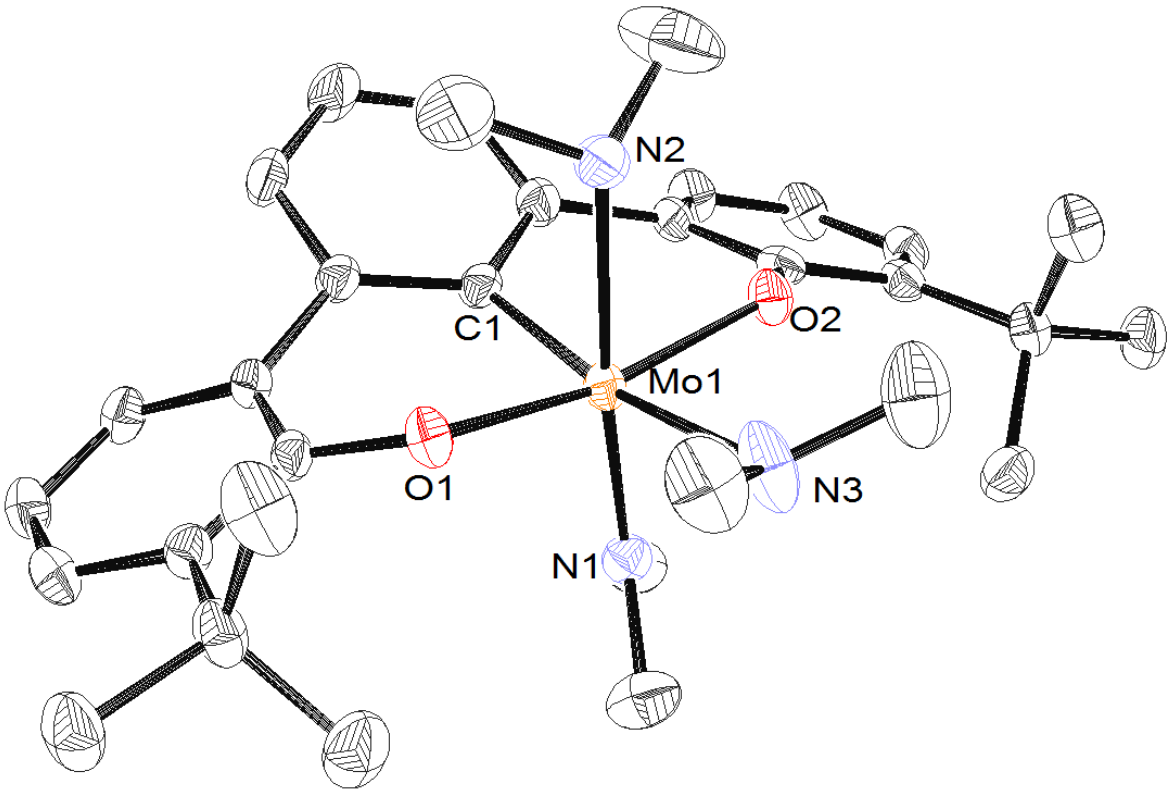


Figure 3-1. ORTEP diagram of [$^t$BuOCO]MoNMe$_2$(HNMe$_2$)$_2$ (**18**). Thermal ellipsoids are displayed at the 50% probability level. Hydrogen atoms and cocrystallized solvent molecules are omitted for clarity.

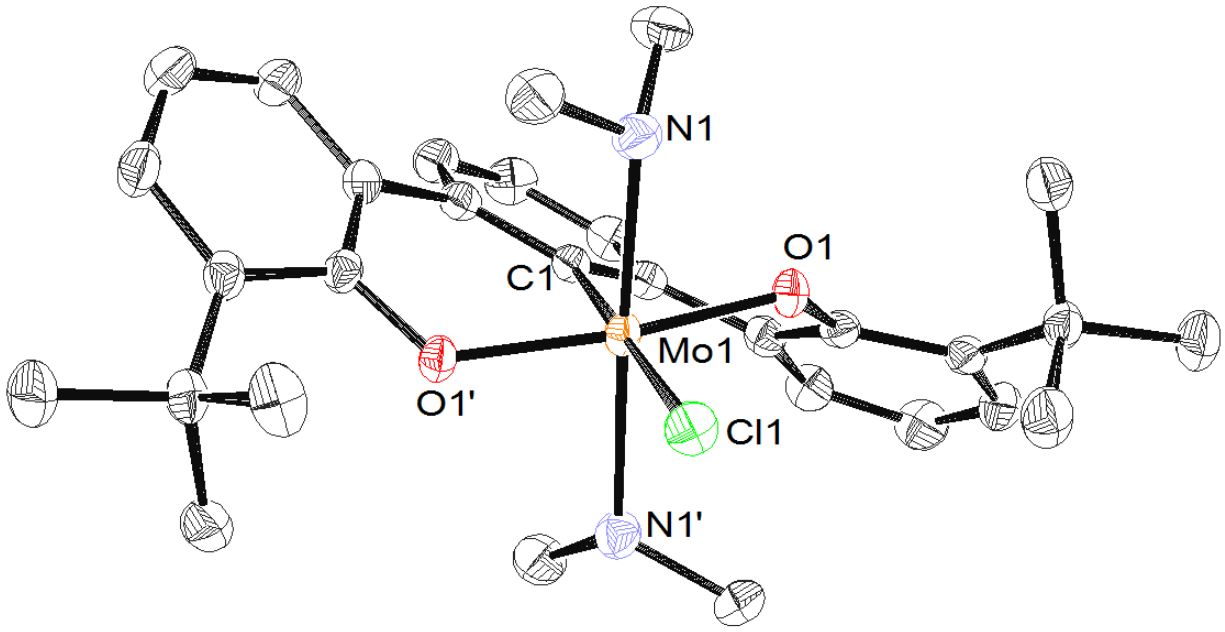


Figure 3-2. ORTEP diagram of [$^t$BuOCO]Mo(HNMe$_2$)$_2$Cl (**19**). Thermal ellipsoids are displayed at the 50% probability level. Hydrogen atoms and cocrystallized solvent molecules are omitted for clarity.

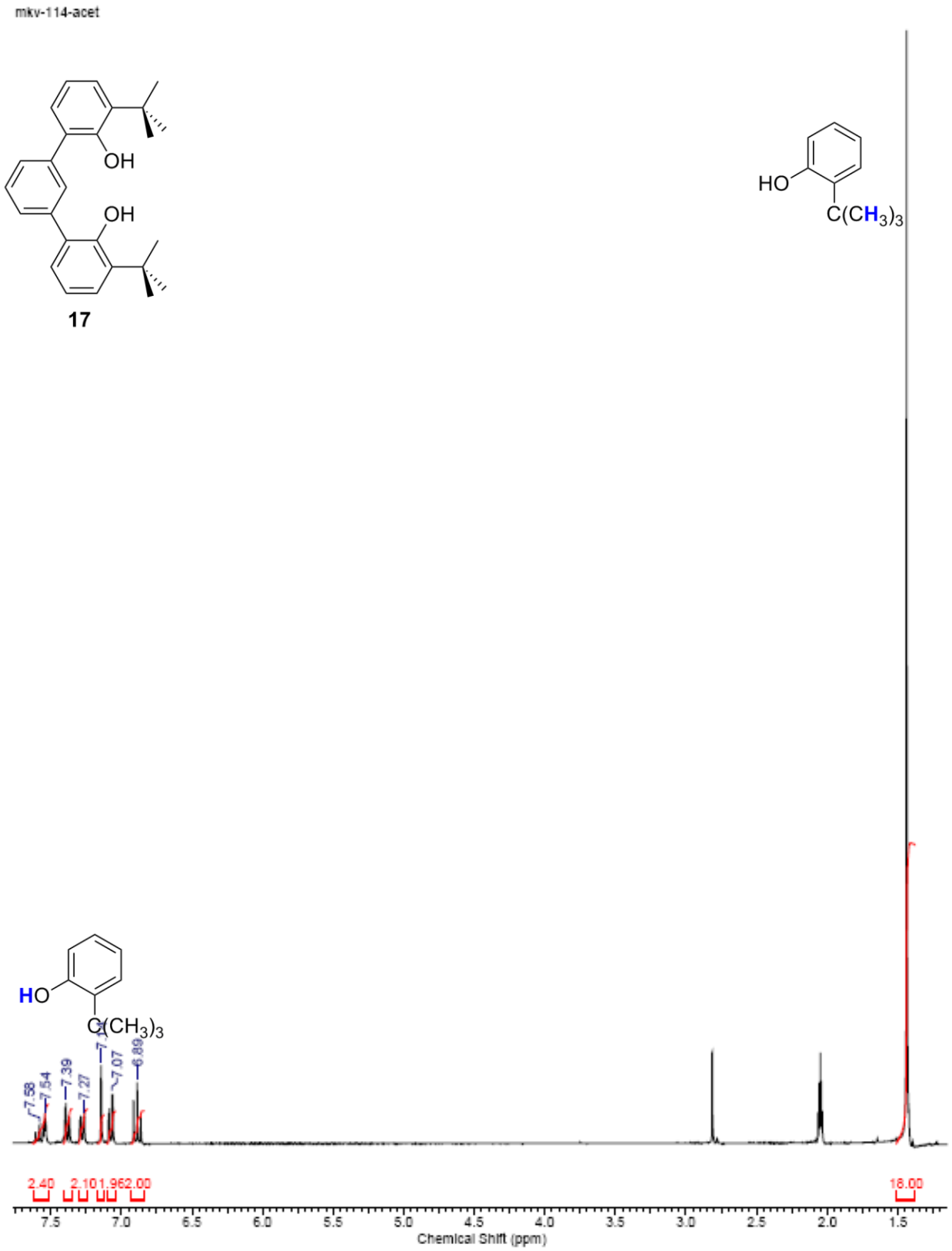


Figure 3-3. $^{1}$H NMR spectrum of [$^{t}$BuOCO]H$_3$ (**17**) in acetone-$d_6$.

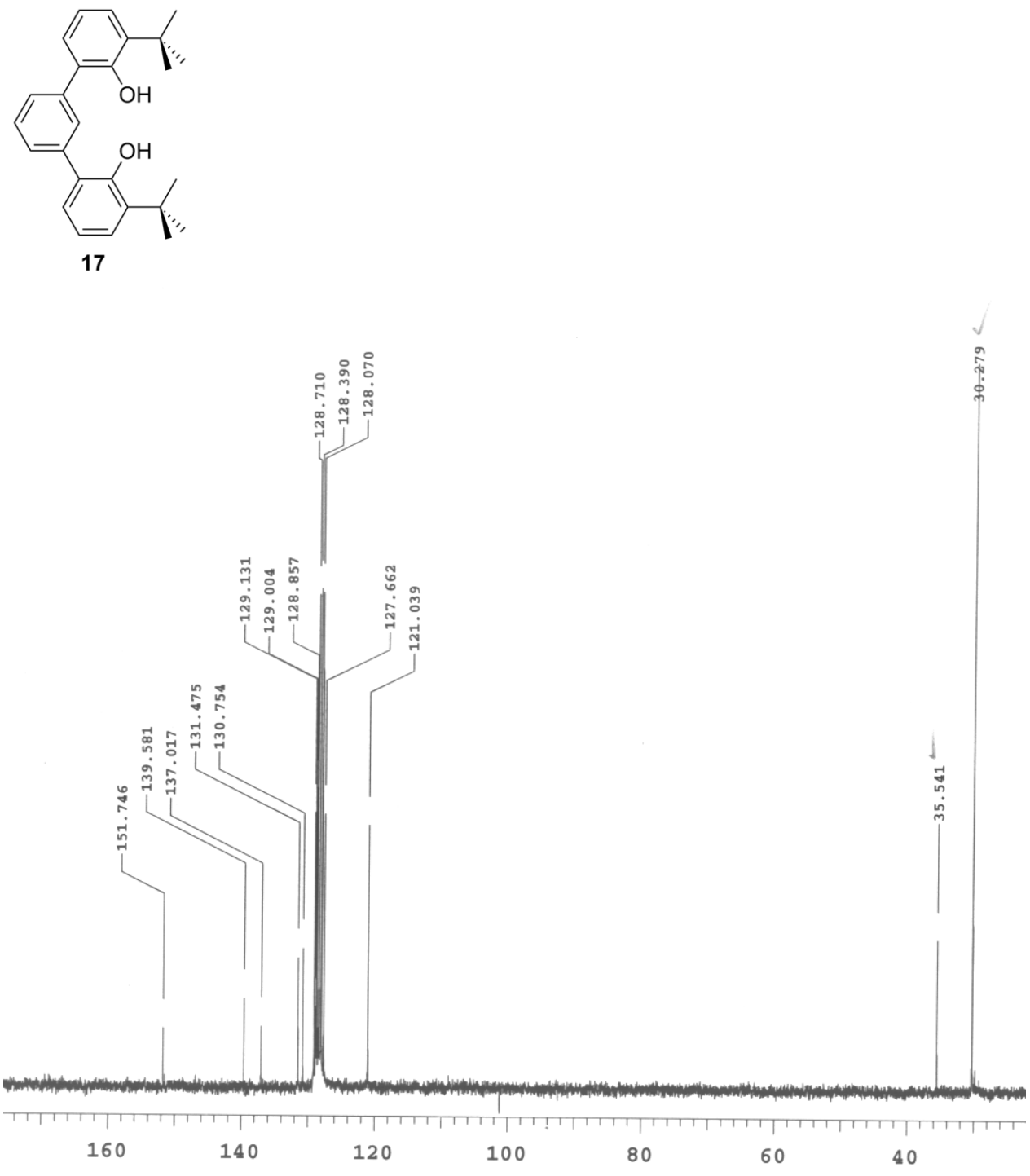


Figure 3-4. $^{13}C$ NMR spectrum of [$^{t}$BuOCO]$H_3$ (**17**) in $C_6D_6$.

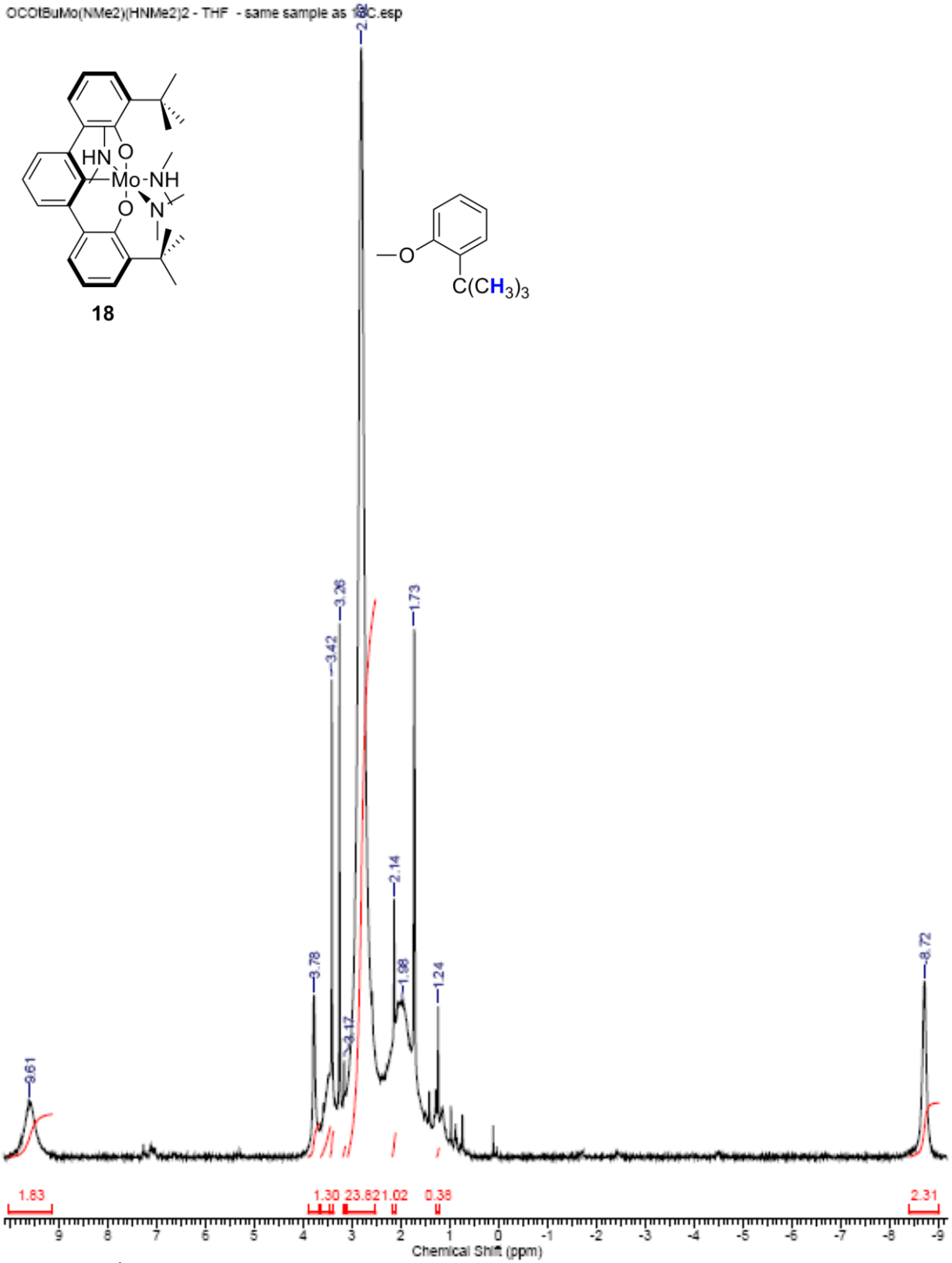


Figure 3-5. $^{1}$H NMR spectrum of [$^{t}$BuOCO]MoNMe$_2$(HNMe$_2$)$_2$ (**18**) in THF-$d_8$.

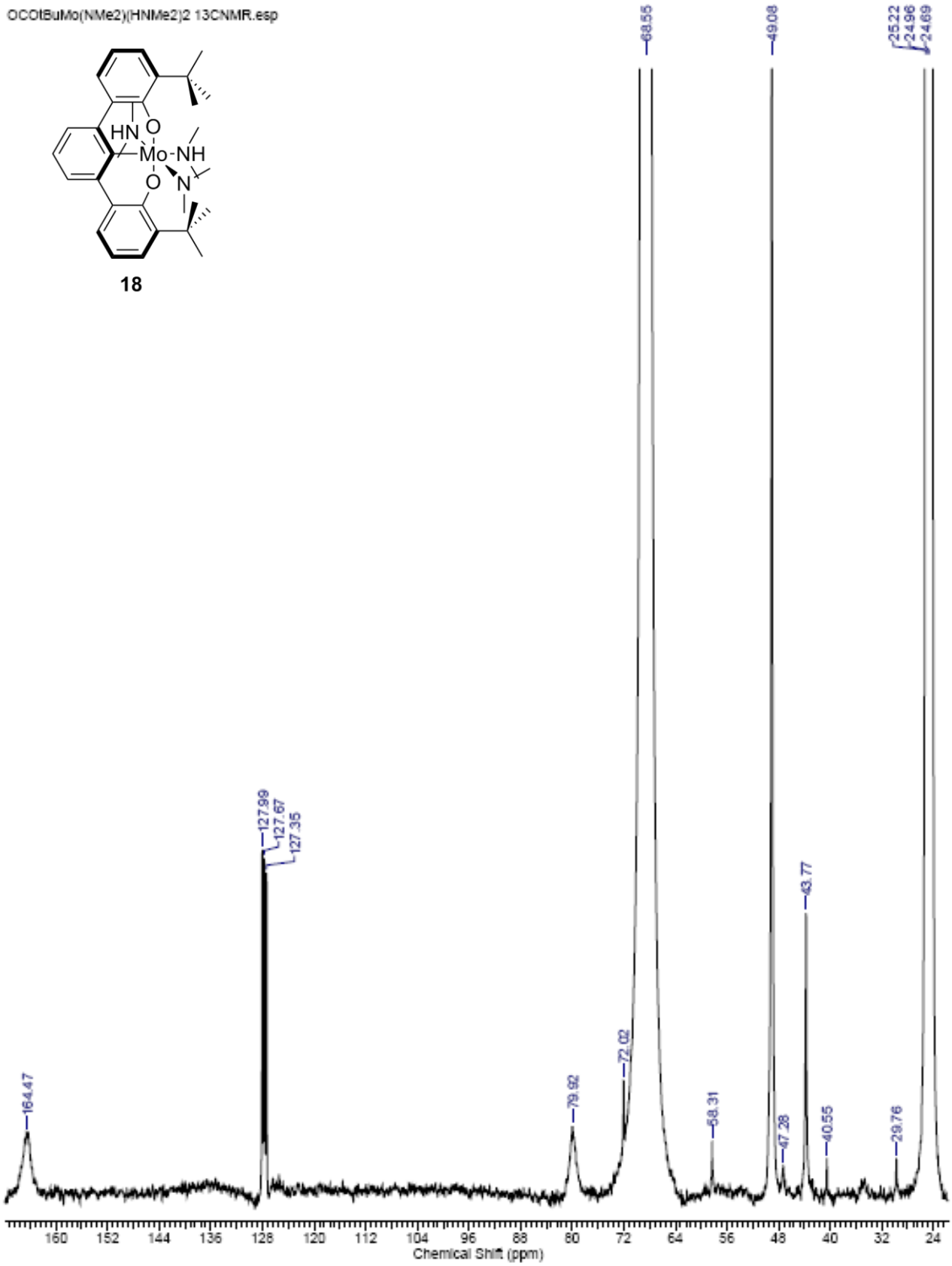


Figure 3-6. $^{13}$C NMR spectrum of [$^{t}$BuOCO]MoNMe$_2$(HNMe$_2$)$_2$ (**18**) in THF-$d_8$.

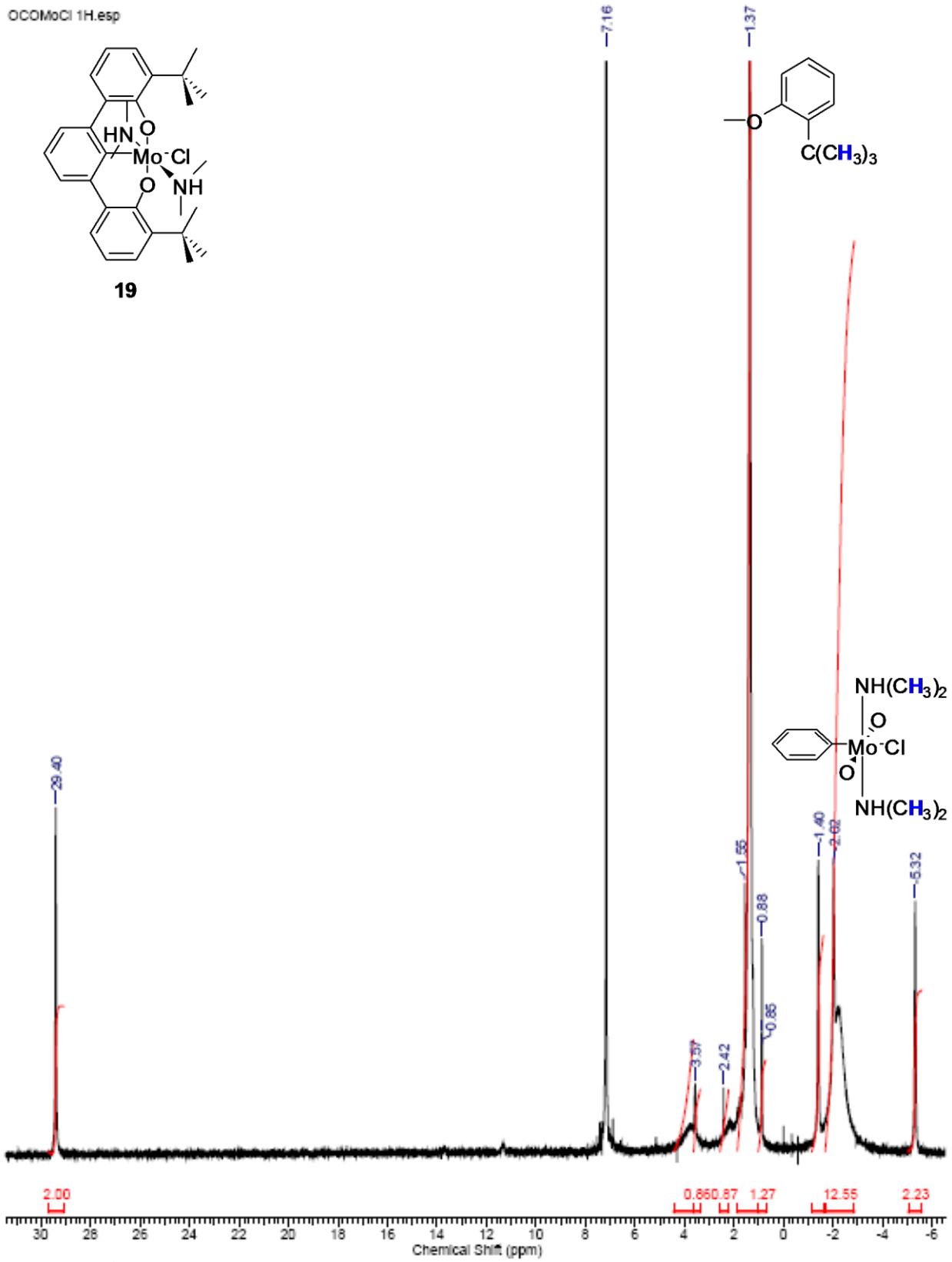


Figure 3-7. $^{1}$H NMR spectrum of [$^{t}$BuOCO]Mo(HNMe$_2$)$_2$Cl (**19**) in $C_6D_6$.

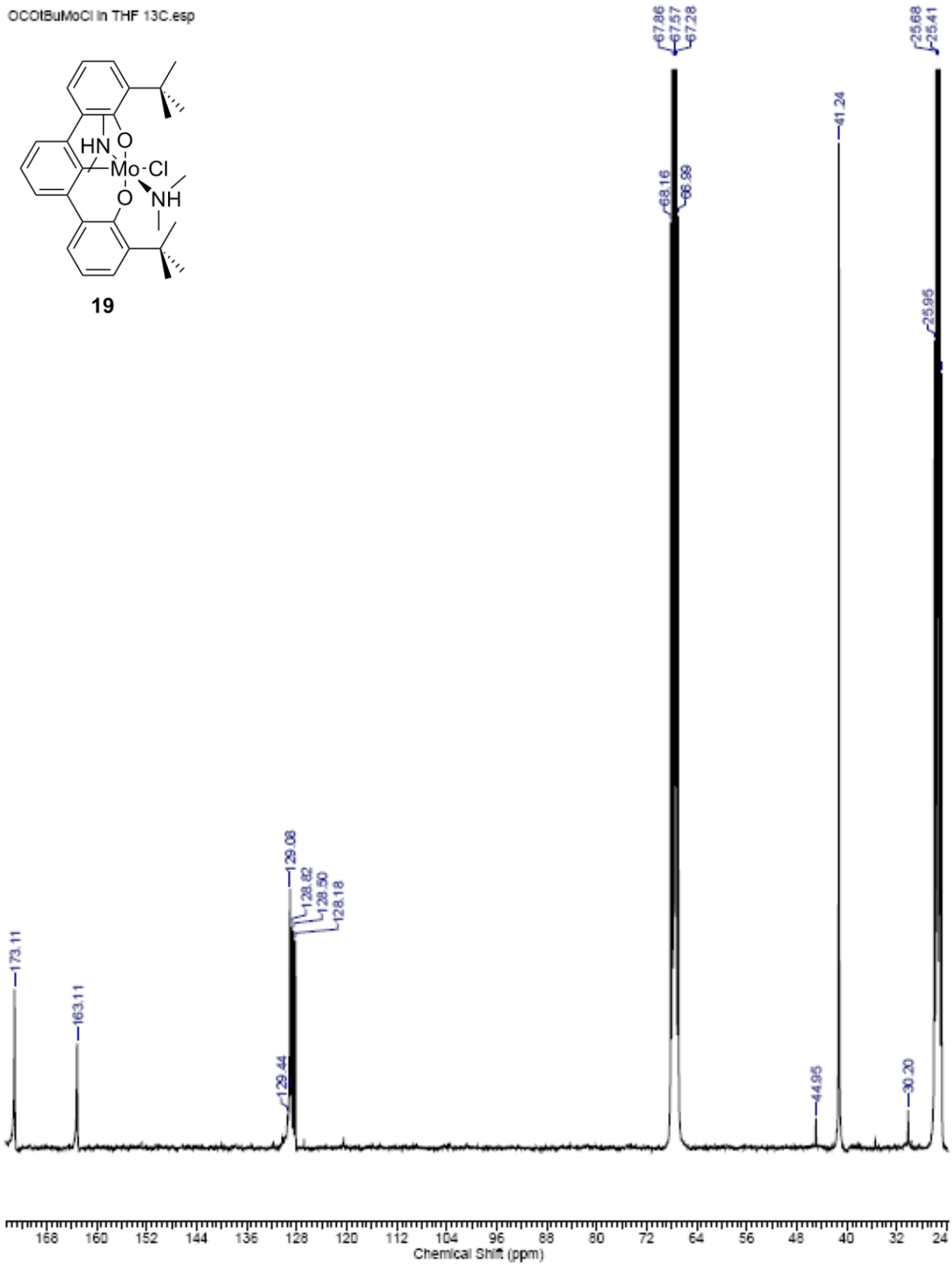


Figure 3-8. $^{13}$C NMR spectrum of [$^{t}$BuOCO]Mo(HNMe$_2$)$_2$Cl (**19**) in THF-$d_8$.

Table 3-1. Selected angles and bond lengths for crystal structures **18** and **19**

| [$^t$BuOCO]MoNMe$_2$(HNMe$_2$)$_2$ (**18**) | | [$^t$BuOCO]Mo(HNMe$_2$)$_2$Cl (**19**) | |
|---|---|---|---|
| Bond Lengths (Å) | | | |
| Mo1-N1 | 1.928(3) | Mo1-O1 | 1.9405(11) |
| Mo1-O1 | 1.997(2) | Mo1-C1 | 2.120(2) |
| Mo1-O2 | 2.014(2) | Mo1-N1 | 2.2245(16) |
| Mo1-C1 | 2.114(3) | Mo1-Cl1 | 2.4829(6) |
| Mo1-N2 | 2.390(3) | | |
| Mo1-N3 | 2.430(3) | | |
| Bond Angles (deg) | | | |
| N1-Mo1-O1 | 98.89(11) | O1-Mo1-C1 | 82.66(3) |
| N1-Mo1-O2 | 94.58(10) | O1-Mo1-N1 | 83.24(5) |
| O1-Mo1-O2 | 166.45(9) | C1-Mo1-N1 | 94.55(4) |
| N1-Mo1-C1 | 98.88(12) | O1-Mo1-Cl1 | 97.34(3) |
| O1-Mo1-C1 | 90.35(11) | C1-Mo1-Cl1 | 180.0 |
| O2-Mo1-C1 | 89.05(11) | N1-Mo1-Cl1 | 85.45(4) |
| N1-Mo1-N2 | 173.45(12) | C6-O1-Mo1 | 128.73(10) |
| O1-Mo1-N2 | 83.68(10) | O1-Mo1-O1’ | 162.32(6) |
| C22-O2-Mo1 | 128.7(2) | N1-Mo1-N1’ | 170.90(8) |
| O2-Mo1-N2 | 82.77(9) | | |
| C1-Mo1-N2 | 87.10(12) | | |
| N1-Mo1-N3 | 92.35(12) | | |
| O1-Mo1-N3 | 89.71(10) | | |
| O2-Mo1-N3 | 88.23(10) | | |
| C1-Mo1-N3 | 168.62(12) | | |
| N2-Mo1-N3 | 81.60(12) | | |
| C12-O1-Mo1 | 129.5(2) | | |

Table 3-2. Crystal data and structure refinement for [$^t$BuOCO]MoNMe$_2$(HNMe$_2$)$_2$ (**18**)

| | |
|---|---|
| identification code | (ac20) |
| empirical formula | $C_{36}H_{57}MoN_3O_4$ |
| formula weight | 691.79 |
| $T$ (K) | 173(2) |
| $\lambda$ (Å) | 0.71073 |
| crystal system | Triclinic |
| space group | P-1 |
| $a$ (Å) | 8.5921(10) |
| $b$ (Å) | 11.8394(14) |
| $c$ (Å) | 18.796(2) |
| $\alpha$ (deg) | 69.916(2) |
| $\beta$ (deg) | 89.349(2) |
| $\gamma$ (deg) | 87.278(2) |
| $V$ (Å$^3$) | 1793.7(4) |
| Z | 2 |
| $\rho_{calcd}$ (Mg mm$^{-3}$) | 1.281 |
| abs coeff (mm$^{-1}$) | 0.406 |
| $F$(000) | 736 |
| crystal size (mm$^3$) | 0.15 x 0.08 x 0.02 |
| $\theta$ range for data collection | 1.08 to 27.50° |
| limiting indices | -11≤h≤11, -13≤k≤15, -24≤l≤19 |
| no. of reflns collcd | 12358 |
| no. of ind reflns ($R_{int}$) | 8062 [R(int) = 0.0364] |
| completeness to $\theta$ = 22.50° | 97.8 % |
| absorption corr | Integration |
| refinement method | Full-matrix least-squares on $F^2$ |
| data / restraints / parameters | 8062 / 0 / 405 |
| GOF[c] on $F^2$ | 0.964 |
| $R1$,[a] $wR2$[b] [I > 2σ] | 0.0477, 0.0957 [5629] |
| $R1$,[a] $wR2$[b] (all data) | 0.0772, 0.1090 |
| largest diff. peak and hole | 0.723 and -0.490 e.Å$^{-3}$ |

R1 = $\sum(||F_o| - |F_c||) / \sum|F_o|$, wR2 = $[\sum[w(F_o^2 - F_c^2)^2] / \sum[w(F_o^2)^2]]^{1/2}$, S = $[\sum[w(F_o^2 - F_c^2)^2] / (n-p)]^{1/2}$, w= $1/[\sigma^2(F_o^2)+(m*p)^2+n*p]$, p = $[\max(F_o^2,0)+ 2* F_c^2]/3$, m & n are constants.

Table 3-3. Crystal data and structure refinement for [$^t$BuOCO]Mo(HNMe$_2$)$_2$Cl (**19**)

| | |
|---|---|
| identification code | (ac12) |
| empirical formula | $C_{42}H_{53}ClMoN_2O_2$ |
| formula weight | 749.25 |
| $T$ (K) | 173(2) |
| $\lambda$ (Å) | 0.71073 |
| crystal system | Orthorhombic |
| space group | Pbcn |
| $a$ (Å) | 10.4875(8) |
| $b$ (Å) | 17.2088(13) |
| $c$ (Å) | 21.1554(15) |
| $\alpha$ (deg) | 90 |
| $\beta$ (deg) | 90 |
| $\gamma$ (deg) | 90 |
| $V$ (Å$^3$) | 3818.1(5) |
| Z | 4 |
| $\rho_{calcd}$ (Mg mm$^{-3}$) | 1.303 |
| abs coeff (mm$^{-1}$) | 0.450 |
| $F$(000) | 1576 |
| crystal size (mm$^3$) | 0.15 x 0.08 x 0.08 |
| $\theta$ range for data collection | 1.93 to 27.49° |
| limiting indices | -13≤h≤10, -22≤k≤21, -27≤l≤25 |
| no. of reflns collcd | 24328 |
| no. of ind reflns ($R_{int}$) | 4392 [R(int) = 0.0493] |
| completeness to $\theta$ = 22.50° | 99.9 % |
| absorption corr | Integration |
| refinement method | Full-matrix least-squares on $F^2$ |
| data / restraints / parameters | 4392 / 0 / 223 |
| GOF[c] on $F^2$ | 1.241 |
| $R1$,[a] $wR2$[b] [I > 2σ] | 0.0263, 0.0771 [3320] |
| $R1$,[a] $wR2$[b] (all data) | 0.0386, 0.0804 |
| largest diff. peak and hole | 0.331 and -0.380 e.Å$^{-3}$ |

R1 = $\sum(||F_o| - |F_c||) / \sum|F_o|$, wR2 = $[\sum[w(F_o^2 - F_c^2)^2] / \sum[w(F_o^2)^2]]^{1/2}$, S = $[\sum[w(F_o^2 - F_c^2)^2] / (n-p)]^{1/2}$, w= $1/[\sigma^2(F_o^2)+(m*p)^2+n*p]$, p = $[max(F_o^2,0)+ 2* F_c^2]/3$, m & n are constants.

LIST OF REFERENCES


1) Errington, R. J.; Shaw, B. L. *J. Organomet. Chem.* **1982**, *238*, 319–325.

2) Crocker, C.; Empsall, H. D.; Errington, R. J.; Hyde, E. M.; McDonald, W. S.; Markham, R.; Norton, M. C.; Shaw, B. L.; Weeks, B. *J. Chem. Soc., Dalton Trans.* **1982**, *7*, 1217–1224.

3) Shaw. B. L.; Errington, J.; McDonald, W. S. *J. Chem. Soc., Dalton Trans.* **1980**, 2312–2314.

4) Shaw, B. L.; Crocker, C.; Errington, R. J.; McDonald, W. S.; Odell, K. J.; Goodfellow, R. J. *J. Chem. Soc., Chem. Commun.* **1979**, 498–499.

5) Shaw, B. L.; Moulton, C. J. *J. Chem. Soc., Dalton Trans*. **1976**, 1020–1024.

6) Slagt, M. Q.; van Zwieten, D. A. P.; Moerkerk, A.; Gebbink, R.; van Koten, G. *Coord. Chem. Rev.* **2004**, *248*, 2275–2282.

7) Slagt, M. Q.; Rodríguez, G.; Grutters, M. M. P.; Gebbink, R. J. M. K.; Klopper, W.; Jenneskens, L. W.; Lutz, M.; Spek, A. L.; van Koten, G. C*hem. Eur. J.* **2004**, *10*, 1331–1344.

8) van der Boom, M. E.; Milstein, D. *Chem. Rev*. **2003**, *103*, 1759–1792.

9) Beletskaya, I. P.; Cheprakov, A. V. *J. Organomet. Chem.* **2004**, *689*, 4055–4082.

10) Albrecht, M.; van Koten, G. *Angew. Chem., Int. Ed*. **2001**, *40*, 3750–3781.

11) Steenwinkel, P.; Gossage, R. A.; van Koten, G. *Chem. Eur. J*. **1998**, *4*, 759–762.

12) Rierveld, M. H. P.; Grove, D. M.; van Koten, G. *New. J. Chem*. **1997**, *21*, (6–7), 751–771.

13) Albrecht, M.; Kocks, B. M.;Spek, A. L.; van Koten, G. *J. Organomet. Chem*. **2001**, *624*, *(1–2)*, 271–286.

14) van der Boom, M. E.; Milstein, D. *Chem. Rev*. **2003**, *103*, 1759-1792.

15) Slagt, M. Q.; Rodrígues, G.; Grutters, M. M. P.; Gebbink, R.J. M. K.; Klopper, W.; Jenneskens, L. W.; Lutz, M.; Spek, A. L.; van Koten, G. *Chem. Eur. J.* **2004**, *10*, 1331-1344.

16) Singleton, J. T. *Tetrahedron*, **2003**, *59*, 1837-1857.

17) Ohff, M.; Ohff, A.; van der Boom, M. E.; Milstein, D. *J. Am. Chem. Soc.* **1997,** *119*, 11687-11688.

18) Morales-Morales, D.; Grause, C.; Kasaoka, K.; Redo´n, R.; Crammer, R. E.; Jensen, C. M. *Inorg. Chem. Acta* **2000,** 300-302, 958–963.

19) Ray, A.; Zhu, K.; Kissin, Y. V.; Cherian, A. E.; Coates, G. W.; Goldman, A. S. *Chem. Commun.* **2005**, 3388-3390.

20) Miyaura, N.; Yamada, K.; Suginome, H.; Suzuki, A. *J. Am. Chem. Soc*. **1985**, *107(4)*, 972-980.

21) Kharasch, M. S.; Engelmann, H.; Mayo, F. R. *J. Org. Chem*. **1938**, *2*, 288.

22) Collman, J. P.; Hegedus, L. S.; Norton, J. R.; Finke, R. G. *Principles and Applications of Organotransition Metal Chemistry*; University Science Books: Mill Valley, CA, **1987**.

23) Parshall, G. W.; Ittel, S. D. *Homogenous Catalysis*; Wiley & Sons, Inc: New York, **1992**.

24) Crabtree, R. H. *The Organometallic Chemistry of the Transition Metals*, 4th Ed, Wiley & Sons, Inc: Hoboken, **2005**.

25) Zucca, A.; Petretto, G. L.; Stoccoro, S.; Cinellu, M. A.; Minghetti, G.; Manassero, M.; Manassero, C.; Male, L.; Albinati, A. *Organometallics* **2006,** *25,* 3996-4001.

26) Zhang, Y.; Wang, J.; Mu, Y.; Shi, Z.; Lu, C.; Zhang, Y.; Qiao, L.; Feng, S. *Organometallics* **2003,** *22,* 4715-4720.

27) Fossey, J. S.; Richards, C. J. *Organometallics* **2002,** *21,* 5259-5264.

28) Morrison, D. L.; Rodgers, P. M.; Chao, Y.; Bruck, M. A.; Grittini, C.; Tajima, T. L; Alexander, S. J.; Rheingold, A. L.; Wigley, D. E. *Organometallics* **1995,** *14,* 2435-2446.

29) Cummins, C. C.; Beachy, M. D.; Schrock, R. R.; Vale, M. G.; Sankaran, V.; Cohen, R. E. *Chem. Mater.* **1991**, *3(6)*, 1153-1163.

30) Wolfe, J. P.; Buchwald, S. L. *J. Org. Chem.* **2000**, *65*, 1144-1157.

31) Wolfe, J. P.; Wagaw, S.; Buchwald, S. L. *J. Am. Chem. Soc.* **1996**, *118*, 7215-7216.

32) Daniele, S.; Hitchcock, P. B.; Lappert, M. F.; Nile, T. A.; Zdanski, C. M. *J. Chem. Soc*., *Dalton Trans*. **2002**, 3980–3984.

33) Chisholm, M. H.; Bradley, D. C. *J. Chem Soc (A)* **1971**, 2741-2743.

34) Ruggli, P.; Prijs, B. *Helvetica Chimica Acta* **1945**, *28*, 674-690.

35) Jones, R. G.; Karmas, G.; Martin Jr, G. A.; Gilman, H. *J. Am. Chem. Soc*. **1956**, *78*, 4285-4286.

36) Bochmann, M.; Wilkinson, G.; Hussain, B.; Motevalli, M.; Hursthouse, M.B. *Polyhedron* **1988,** *7,* 1363-1370.

37) Chisholm, M. H.; Hammond, C. E.; Huffman, J. C. *Polyhedron* **1989**, *8*, 129-131.

38) Chisholm, M. H.; Reichert, W. W.; Thornton, P. *J. Am. Chem. Soc.* **1978**, *100(9)*, 2744-2748.

39) Greco, G. E.; Schrock, R. R. *Inorg. Chem.* **2001,** *40*, 3850-3860.

40) Listemann, M. L.; Schrock, R. R.; Dewan, J. C.; Kolodziej, R. M. *Inorg. Chem.* **1988,** *27(2)*, 264-271.

41) Yasuda, H.; Nakayama, Y.; Takei, K.; Nakamura, A.; Kai, Y.; Kanehisa, N. *J. Organometallic Chem.* **1994,** *473,* 105-116.

42) Zhang, Y.; Wang, J.; Mu, Y.; Shi, Z.; Lu, C.; Zhang, Y.; Qiao, L.; Feng, S. *Organometallics,* **2003**, *22,* 3877-3883.

43) Du, C, J, F,; Hart, H.; Ng, K, K. D. *J. Org. Chem.* **1986**, *51*, 3162-3165.

# BIOGRAPHICAL SKETCH

Adam Rand Carlson was born in 1979 in Cedar Rapids, Iowa. He graduated with a B.A. in chemistry from The University of Northern Iowa in 2003. After graduation Adam spent two years doing masters research in analytical chemistry at the University of Northern Iowa. He came to the University of Florida in 2005 and joined the Veige Group. Upon completion of his M.S. program, Adam moved to San Antonio, Texas and is currently employed with D.R. Horton.